Passive modelling of the electrodynamic loudspeaker: from the Thiele-Small model to nonlinear Port-Hamiltonian Systems

Antoine Falaize, Thomas Hélie

Passive modelling of the electrodynamic loudspeaker: from the Thiele-Small model to nonlinear Port-Hamiltonian Systems

Version Jul 21, 2018

Antoine Falaize[1], Thomas Hélie[2]
[1] M2N team, Laboratory LaSIE (UMR 7356), CNRS, Université de La Rochelle, 17042 La Rochelle cedex 1, France. antoine.falaize@univ-lr.fr
[2] CNRS, S3AM team, Laboratory STMS (UMR 9912), IRCAM-CNRS-SU, 1, place Igor Stravinsky, 75004 Paris, France. thomas.helie@ircam.fr

Abstract

The electrodynamic loudspeaker couples mechanical, magnetic, electric and thermodynamic phenomena. The Thiele/Small (TS) model provides a low frequency approximation, combining passive linear (multi-physical or electric-equivalent) components. This is commonly used by manufacturers as a reference to specify basic parameters and characteristic transfer functions. This paper presents more refined nonlinear models of electric, magnetic and mechanical phenomena, for which fundamental properties such as passivity and causality are guaranteed. More precisely, multi-physical models of the driver are formulated in the core class of port-hamiltonian systems (PHS), which satisfies a power balance decomposed into conservative, dissipative and source parts. First, the TS model is reformulated as a linear PHS. Then, refinements are introduced, step-by-step, benefiting from the component-based approach allowed by the PHS formalism. Guaranteed-passive simulations are proposed, based on a numerical scheme that preserves the power balance. Numerical experiments are presented throughout the paper, for each refinement. They are in accordance with results in the literature.

1 Introduction

The electrodynamic loudspeaker is a non ideal transducer. Its dynamics is governed by intricate multi-physical phenomena (mechanical, magnetic, electric and thermodynamic), a part of which involves nonlinearities responsible for audio distortions [26, 36, 6]. As a first example, the viscoelastic properties of the suspension material result in long-term memory (linear) and hardening spring effect (nonlinear). Second, the voice-coil includes a solid iron core charged by a strong magnet. This is responsible for long-term memory due to eddy current losses (linear) and ferromagnetic saturation (nonlinear). Third, the resistance of the coil wire converts a part of electrical power into heat. This modifies material properties and, eventually, can cause irreversible damages. Such phenomena must be modeled and considered in the design of real-time distortion compensation [46, 22, 3, 14] and that of burn-out protection [36, 47].

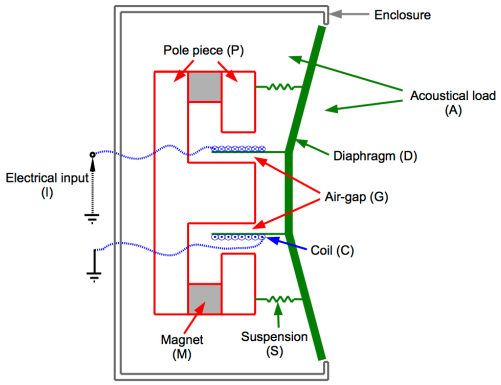

Figure 1: Schematic of the electrodynamic loudspeaker and components labels.

The basic reference model of the electrodynamic loudspeaker is that of Thiele-Small [48, 49, 43, 44]. It combines *passive linear models of elementary physical components* (see figure 1) and provides a low-frequency linear time-invariant approximation for low-amplitude excitation on short period. This (multi-physical or electric-equivalent) parametric model is commonly used by manufacturers as a reference to specify basic parameters and characteristic transfer functions.

Various refinements of this reference model have been proposed, both in the frequency domain and the time domain [10, 32, 25, 52, 51, 1, 6]. In particular, the lumped-parameter approach [24, 26, 36, 4] consists in modeling the dependence of Thiele-Small parameters on some selected physical quantities (*e.g.* position-dependent stiffness). However, fundamental physical properties such as causality and passivity are usually not guaranteed by these refinements, and their physical interpretation is not always obvious. Obviously, this is also the case for *gray-box*

modelling based on Volterra and Wiener/Volterra series [23, 5, 30, 7] or nonlinear ARMAX [45]).

The elementary phenomena that are considered in this paper are concerned with mechanical, magnetic and electric phenomena, as well as their coupling. They are known to be responsible for significant audio distortions (see *e.g.* [26, 36] and references therein). We restart from the Thiele-Small model and propose several refinements, based on nonlinear lumped-parameter models, that preserve passivity. To this end, the proposed models are all recast as *port-Hamiltonian systems* [35, 41, 12], which are state-space representations that satisfy a power balance structured into conservative, dissipative and external(/source) parts. For all these multi-physical passive nonlinear models, guaranteed-passive simulations are proposed. They are based on a numerical method that preserves the power balance and its structure in the discrete-time domain, from which passivity and stability properties stem.

This paper is structured as follows. Section 2 presents the list of the physical phenomena and multi-physical couplings that are considered in this paper. Section 3 introduces (a slightly refined version of) the Thiele-Small model (model 0) which recast as a Port-Hamiltonian Systems. This model 0 serves as a basis to elaborate two refined loudspeaker models (model 1 and model 2). Section 4 focuses on refinements of the mechanical part (model 1). Section 5 focuses on refinements of the electromagnetic part (model 2). These passive models can straightforwardly be combined to include all these refinements. Simulation results are presented throughout the paper, focusing on the effect of each phenomena, separately.

2 Refinements under consideration for multi-physical couplings and phenomena

An important origin of nonlinearities lies in the coupling of multi-physical phenomena that involve factors depending on the driver state. Also, mechanical, magnetic and electric phenomena involve nonlinearities due to the non ideal design of materials and components.

2.1 Coupling phenomena

First, the electromechanical coupling (back e.m.f. and Lorentz force) depends on the coil (`C`) position with respect to the pole piece (`P`).

Phenomenon 1 (Position-dependent force factor)**.** *The fraction of coil wire subjected to the magnetic flux in the air gap depends on the coil position. This leads to consider a position-dependent effective wire length $\ell(q_{\mathtt{D}})$ in the force factor B_ℓ (see e.g. [26, figure 5]).*

Second, the coil acts as an electromagnet that modifies the magnetic flux in the pole piece.

Phenomenon 2 (Flux-dependent force factor)**.** *The magnetic flux $\phi_{\mathtt{PG}}$ common to the air gap (`G`) and pole piece (`P`) depends on the magnetic flux induced in the coil due to an applied voltage (Faraday's law of induction). This leads to consider a flux-dependent magnetic induction $B(\phi_{\mathtt{PG}})$ in the force factor B_ℓ (see e.g.[26, figure 8]).*

Third, the electromagnetic coupling (coil inductive effect) also depends on the coil (`C`) position with respect to the pole piece (`P`).

Phenomenon 3 (Position-dependent inductance)**.** *The fraction of the coil core occupied by the pole piece depends on the coil position $q_{\mathtt{D}}$ (see e.g. [26, figure 6]). This leads to consider a position-dependent electromagnetic coupling between the electrical domain (`C`) and the magnetic domain (`P`).*

2.2 Mechanical phenomena

The suspension (`S`) includes the spider and surround, which are usually made of polymer and rubber, respectively (see [36, §2.3.1], [26, §3.1.1]). The mechanical properties of those materials are responsible for two phenomena that cannot be described by a standard (linear) stiffness.

Phenomenon 4 (Viscoelasticity)**.** *The materials used for the suspension (`S`) exhibit combination of the behaviors of elastic solids and viscous fluid [27, §1.2], inducing long time shape memory (creep effect, see e.g. [27, figure 1] and [37, figure 11]).*

Phenomenon 5 (Hardening suspension)**.** *The materials used for the suspension (`S`) exhibit nonlinear stress–strain characteristics so that the restoring force is not proportional to the elongation [26, 1], with maximal instantaneous excursion $q_{\mathtt{sat}}$ that corresponds to the breakdown of the material.*

2.3 Electromagnetic phenomena

The core of the coil (`C`) is the ferromagnetic pole piece (`P`) surrounded by air (`G`), as shown in figure 1, inducing a coupling between the magnetic flux in the coil and that common to the magnet (`M`), air gap (`G`) and the pole piece (`P`). The electromagnetic properties of the latter is responsible for two nonstandard phenomena.

Phenomenon 6 (Ferromagnetic saturation)**.** *The materials used for the pole piece `P` exhibit nonlinear magnetic excitation–induction curve so that the equivalent current in the coil is not proportional to*

its magnetic flux. A maximal magnetic flux $\phi_{\mathtt{sat}}$ is reached (flux saturation), corresponding to the global alignment of the microscopic magnetic moments (see [17, §1], [16]).

Phenomenon 7 (Eddy-currents losses)**.** *Most of the magnetic materials (iron, cobalt, etc.) possess high electric conductivity. The application of a variable magnetic induction induces currents, namely eddy-currents, in a plane orthogonal to the field lines (see [38, §1.1.2]). This has three effects: (i) a power is dissipated due to the natural resistivity of the material (Joule effect), (ii) eddy-currents induces their own magnetic field (added inductive effect), and (iii) they oppose to the original induction (Lens's law), which pushes the field lines toward the boundary (magnetic skin effect).*

In this work, we propose passive guaranteed models of these phenomena, based on the Port-Hamiltonian Systems formalism described in the next section.

3 The Thiele-Small model revisited in the Port-Hamiltonian formalism

This section is devoted to the construction of the base model (model 0) that is progressively refined in the remaining of the paper. First, an overview of the functioning of the electrodynamic loudspeaker is presented and the standard Thiele-Small modeling is recalled. Second, the port-Hamiltonian framework is recalled. Third, the Thiele-Small modeling is refined to cope with the force factor modulation (phenomenon 1) and the result is recast as a port-Hamiltonian system (model 0). Finally, simulation results are shown.

3.1 Standard Thiele/Small model

The basic functioning of a boxed loudspeaker such as the one depicted in figure 1 is as follows. A voice-coil (C) is immersed in a magnetic field imposed by a permanent magnet (M) in the air gap (G) of a magnetic path (pole piece P). The coil (C) is glued to a large diaphragm (D) which is maintained by a flexible suspension (S). An input tension imposed to the coil (C) induces a flow of electric charges through the wire (a current due to the self inductance of the coil). Each moving charge in the magnetized air gap imposes a force, orthogonal to the charge velocity and the magnetic induction field (Lorentz force). The resultant force experienced by the diaphragm is the sum of (i) the Lorentz force, (ii) the force due to the suspension (S) (which includes spring effect and friction losses) and (iii) the acoustical load (A).

The standard description of the dynamics of this system is referred as the Thiele-Small modeling, introduced in the early seventies [48, 49, 43, 44]. The electrical part (C) includes the electrical resistance of the coil wire $R_{\mathtt{C}}$ and the linear approximation of the coil behavior with inductance $L_{\mathtt{C}}$. The mechanical part (C,D,S,A) is modeled as a damped harmonic oscillator with mass $M_{\mathtt{CDA}}$ (coil, diaphragm and additional mass due to acoustic radiation), linear approximation of the spring effect $K_{\mathtt{SA}}$ (suspension and additional stiffness due to air compression in the enclosure) and fluid-like damping with coefficient $R_{\mathtt{SA}}$ (frictions and acoustic power radiation). The magnetic part (M,P,G,C) reduces to a constant force factor B_ℓ.

The corresponding set of ordinary differential equations are derived by applying Kirchhoff's laws to the electrical part (C) and Newton's second law to the mechanical part (D,S,A):

$$v_{\mathtt{I}}(t) = v_{\mathcal{L}}(t) + R_{\mathtt{C}}\, i_{\mathtt{C}}(t) + L_{\mathtt{C}}\frac{\mathtt{d}i_{\mathtt{C}}(t)}{\mathtt{d}t}, \quad (1)$$

$$M_{\mathtt{CDA}}\frac{\mathtt{d}^2 q_{\mathtt{D}}(t)}{\mathtt{d}t^2} = f_{\mathcal{L}}(t) - R_{\mathtt{SA}}\frac{\mathtt{d}q_{\mathtt{D}}(t)}{\mathtt{d}t} - K_{\mathtt{SA}}\, q_{\mathtt{D}}(t), \quad (2)$$

with $v_{\mathtt{I}}$ the input voltage, $i_{\mathtt{C}}$ the coil current and $q_{\mathtt{D}}$ the diaphragm's displacement from equilibrium. The electro-mechanical coupling terms are the back electromotive force (tension) $v_{\mathcal{L}} = B_\ell\, \frac{\mathtt{d}q_{\mathtt{D}}}{\mathtt{d}t}$ and the Lorentz force $f_{\mathcal{L}} = B_\ell\, i_{\mathtt{C}}$.

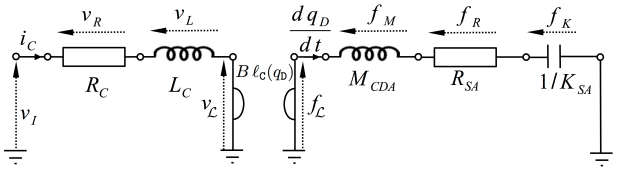

Figure 2: Equivalent circuit of the model 0 with direct electromechanical analogy (force↔voltage, velocity↔current). It corresponds to the Thiele-Small model (1)-(2) with position-dependent electromechanical coupling (phenomenon 1) that restores the gyrator (35) with the force factor $B\,\ell_{\mathtt{C}}(q_{\mathtt{D}})$ for the effective wire length $\ell_{\mathtt{C}}(q_{\mathtt{D}})$ in (6).

3.2 Port-Hamiltonian formalism

The port-Hamiltonian (pH) formalism introduced in the 90's [35] is a modular framework for the passive-guaranteed modeling of open dynamical systems. In this paper, we consider the following class formulated as a differential algebraic state-space representation, as in [13]. (multi-physical component-based)

Definition 1 (Port-Hamiltonian Systems (PHS))**.** *The class of PHS under consideration is that of differential algebraic state-space representations with input*

$\mathbf{u} \in \mathbb{R}^{n_\mathbf{y}}$, *state* $\mathbf{x} \in \mathbb{R}^{n_\mathbf{x}}$, *output* $\mathbf{y} \in \mathbb{R}^{n_\mathbf{y}}$, *that are structured according to energy flows and described by (see [13] for details and [35, 41, 12] for more general formulations of PHS):*

$$\begin{pmatrix} \frac{\mathrm{d}\mathbf{x}}{\mathrm{d}t} \\ \hline \mathbf{w} \\ \hline \mathbf{y} \end{pmatrix} = \underbrace{\left(\begin{array}{c|c|c} \mathbf{J}_\mathbf{x} & -\mathbf{K} & \mathbf{G}_\mathbf{x} \\ \hline \mathbf{K}^\intercal & \mathbf{J}_\mathbf{w} & \mathbf{G}_\mathbf{w} \\ \hline -\mathbf{G}_\mathbf{x}{}^\intercal & -\mathbf{G}_\mathbf{w}{}^\intercal & \mathbf{J}_\mathbf{y} \end{array}\right)}_{\mathbf{J}} \begin{pmatrix} \nabla \mathrm{H}(\mathbf{x}) \\ \hline \mathbf{z}(\mathbf{w}) \\ \hline \mathbf{u} \end{pmatrix}, \quad (3)$$

where $\mathbf{w} \in \mathbb{R}^{n_\mathbf{w}}$ *stands for dissipation variables with dissipation law* $\mathbf{z}(\mathbf{w}) \in \mathbb{R}^{n_\mathbf{w}}$, $\mathrm{H}(\mathbf{x}) \in \mathbb{R}_+$ *is the energy storage function (or Hamiltonian) with gradient* $(\nabla \mathrm{H}(\mathbf{x}))_i = \frac{\partial \mathrm{H}}{\partial x_i}$, $\mathbf{K} \in \mathbb{R}^{n_\mathbf{x} \times n_\mathbf{w}}$, $\mathbf{G}_\mathbf{x} \in \mathbb{R}^{n_\mathbf{x} \times n_\mathbf{y}}$, $\mathbf{G}_\mathbf{w} \in \mathbb{R}^{n_\mathbf{w} \times n_\mathbf{y}}$, *and where*

(i) the storage function $\mathrm{H}(\mathbf{x})$ *is semi-positive definite* $\mathrm{H}(\mathbf{x}) \geq 0$ *with* $\mathrm{H}(0) = 0$ *and positive definite Hessian matrix* $[\mathcal{H}_\mathrm{H}(\mathbf{x})]_{i,j} = \frac{\partial^2 \mathrm{H}}{\partial x_i, \partial x_j}(\mathbf{x})$,

(ii) the dissipation law $\mathbf{z}(\mathbf{w})$ *is null at origin* $\mathbf{z}(0) = 0$ *with positive definite Jacobian matrix* $[\mathcal{J}_\mathbf{z}(\mathbf{w})]_{i,j} = \frac{\partial z_i}{\partial w_j}(\mathbf{w})$, *implying that the dissipated power is* $\mathrm{P_D}(\mathbf{w}) = \mathbf{z}(\mathbf{w})^\intercal \mathbf{w} \geq 0$, $\mathrm{P_D}(0) = 0$,

(iii) $\mathbf{J}_\mathbf{x} \in \mathbb{R}^{n_\mathbf{x} \times n_\mathbf{x}}$, $\mathbf{J}_\mathbf{w} \in \mathbb{R}^{n_\mathbf{w} \times n_\mathbf{w}}$ *and* $\mathbf{J}_\mathbf{y} \in \mathbb{R}^{n_\mathbf{y} \times n_\mathbf{y}}$ *are skew-symmetric matrices, so that* $\mathbf{J}^\intercal = -\mathbf{J}$.

System (3) proves passive for the *outgoing* power $\mathrm{P_S} = \mathbf{u}^\intercal \mathbf{y}$ according to the following power balance:

$$\begin{pmatrix} \nabla \mathrm{H}(\mathbf{x}) \\ \hline \mathbf{z}(\mathbf{w}) \\ \hline \mathbf{u} \end{pmatrix}^\intercal \begin{pmatrix} \frac{\mathrm{d}\mathbf{x}}{\mathrm{d}t} \\ \hline \mathbf{w} \\ \hline \mathbf{y} \end{pmatrix} = \frac{\mathrm{dH}}{\mathrm{d}t}(\mathbf{x}) + \underbrace{\mathrm{P_D}(\mathbf{w})}_{\geq 0} + \mathrm{P_S} = 0. \quad (4)$$

This proves the passivity and hence the asymptotic stability of (3) in the sense of Lyapunov [42, §4].

3.3 The Thiele-Small model as a modulated PHS

The Thiele-Small modeling from section 3.1 can be regarded as the interconnection of a resistance-inductance circuit with a mass-spring-damper system, through a gyrator that describes the reversible energy transfer from the electrical domain to the mechanical domain as depicted in figure 2 and detailed in B.2.

Description This system includes $n_\mathbf{x} = 3$ storage components (inductance $L_\mathtt{C}$, mass $M_\mathtt{CDA}$ and stiffness $K_\mathtt{SA}$), $n_\mathbf{w} = 2$ dissipative components (electrical resistance $R_\mathtt{C}$ and mechanical damping $R_\mathtt{SA}$) and $n_\mathbf{y} = 1$ port (electrical input $v_\mathtt{I}$). The state $\mathbf{x} = (\phi_\mathtt{C}, p_M, q_\mathtt{D})^\intercal$ consists of the magnetic flux in the coil $\phi_\mathtt{C}$, mass momentum $p_\mathtt{M} = M_\mathtt{CDA} \frac{\mathrm{d}q_\mathtt{D}}{\mathrm{d}t}$ and diaphragm position $q_\mathtt{D}$. The Hamiltonian is the sum of the electrodynamic energy $\mathrm{H_L}(x_1) = \frac{x_1^2}{2L_\mathtt{C}}$, the kinetic energy $\mathrm{H_M}(x_2) = \frac{x_2^2}{2M_\mathtt{CDA}}$ and the potential energy $\mathrm{H_K}(x_3) = K_\mathtt{SA} \frac{x_3^2}{2}$. The dissipation variable is $\mathbf{w} = (i_\mathtt{C}, \frac{\mathrm{d}q_\mathtt{D}}{\mathrm{d}t})^\intercal$ with linear dissipation law $\mathbf{z}(\mathbf{w}) = \mathrm{diag}(R_\mathtt{C}, R_\mathtt{SA})\, \mathbf{w}$.

Storage	
State: $\mathbf{x} = (\phi_\mathtt{C}, p_\mathtt{M}, q_\mathtt{D})^\intercal$	Energy: $\mathrm{H}(\mathbf{x}) = \frac{x_1^2}{2L_\mathtt{C}} + \frac{x_2^2}{2M_\mathtt{CDA}} + K_\mathtt{SA} \frac{x_3^2}{2}$
Dissipation	
Variable: $\mathbf{w} = \left(i_\mathtt{C}, \frac{\mathrm{d}q_\mathtt{D}}{\mathrm{d}t}\right)^\intercal$	Law: $\mathbf{z}(\mathbf{w}) = \mathrm{diag}(R_\mathtt{C}, R_\mathtt{SA})\, \mathbf{w}$
Ports	
Input: $\mathbf{u} = (v_\mathtt{I})^\intercal$	Output: $\mathbf{y} = (-i_\mathtt{C})^\intercal$
Structure	
$\mathbf{J}_\mathbf{x} = \begin{pmatrix} 0 & -B\ell_\mathtt{C}(x_3) & 0 \\ B\ell_\mathtt{C}(x_3) & 0 & -1 \\ 0 & 1 & 0 \end{pmatrix}$, $\mathbf{K} = \begin{pmatrix} 1 & 0 \\ 0 & 1 \\ 0 & 0 \end{pmatrix}$, $\mathbf{G}_\mathbf{x} = \left(1, 0, 0\right)^\intercal$, $\mathbf{J}_\mathbf{w} = \mathbb{0}_{2\times 2}$, $\mathbf{G}_\mathbf{w} = \mathbb{0}_{2\times 1}$, $\mathbf{J}_\mathbf{y} = 0$.	

Table 1: Port-Hamiltonian formulation (3) for the Thiele-Small structure with position-dependent force factor (model 0) as depicted in figure 2, with magnetic flux in the coil $\phi_\mathtt{C}$, diaphragm position $q_\mathtt{D}$ and momentum $p_M = M_\mathtt{CDA} \frac{\mathrm{d}q_\mathtt{D}}{\mathrm{d}t}$. The position-dependent effective wire length $\ell_\mathtt{C}(q_\mathtt{D})$ is defined in (6). Physical parameters are given in table 6.

Position-dependent force factor (model 0) The gyrator that restores the Lorentz force $f_\mathcal{L}$ with corresponding back electromotive force $v_\mathcal{L}$ is given by (see (35) in appendix B.2)

$$\begin{pmatrix} v_\mathcal{L} \\ f_\mathcal{L} \end{pmatrix} = \begin{pmatrix} 0 & -B\,\ell_\mathtt{C} \\ B\ell_\mathtt{C} & 0 \end{pmatrix} \begin{pmatrix} i_\mathtt{C} \\ \mathrm{v_C} \end{pmatrix}, \quad (5)$$

with coil velocity $\mathrm{v_C} = \frac{\mathrm{d}q_\mathtt{D}}{\mathrm{d}t}$ and $\ell_\mathtt{C}$ the length of coil wire effectively subjected to the magnetic field B. The latter depends on the coil position (phenomenon 1, see [36, figures 2.5–2.8] and [26, figure 5]). We propose a parametric plateau function $\ell_\mathtt{C} : q_\mathtt{D} \mapsto \ell_\mathtt{C}(q_\mathtt{D})$:

$$\ell_\mathtt{C}(q_\mathtt{D}) = {\ell_\mathtt{C}}^0 \frac{1 + \exp(-P_\ell)}{1 + \exp\left(P_\ell \left(\left(\frac{q_\mathtt{D}}{Q_\ell}\right)^2 - 1\right)\right)}, \quad (6)$$

where ${\ell_\mathtt{C}}^0$ is the total length of the coil, Q_ℓ describes the overhang of the coil with respect to the magnetic path (see figure 3a and [26, § 3.1.2]), and P_ℓ is a shape parameter (see figure 3b).

Port-Hamiltonian formulation The model 0 is recast as a port-Hamiltonian system (3) by rewriting

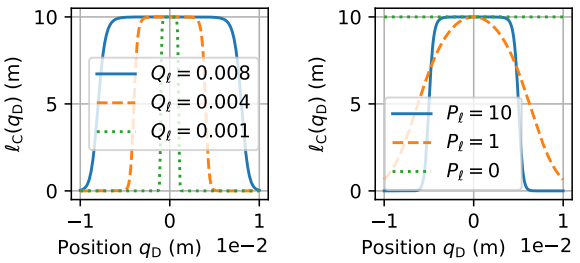

(a) Effect of the overhang parameter Q_ℓ with $P_\ell = 10$.

(b) Effect of the shape parameter P_ℓ with $Q_\ell = 5$mm.

Figure 3: Effective length of coil wire ℓ_C subjected to the magnetic field B as defined in (6), with coil position q_D and total wire length ${\ell_C}^0 = 10$m. Notice $P_\ell = 0$ corresponds to $\ell_C = {\ell_C}^0$, $\forall q_D \in \mathbb{R}$.

the Thiele-Small model (1)–(2) for the above definitions:

$$\begin{aligned} \tfrac{\mathrm{d}x_1}{\mathrm{d}t} &= -B\,\ell_C(x_3)\,\tfrac{\partial \mathrm{H}}{\partial x_2}(x_2) - z_1(w_1) + u_1, \\ \tfrac{\mathrm{d}x_2}{\mathrm{d}t} &= B\,\ell_C(x_3)\,\tfrac{\partial \mathrm{H}}{\partial x_1}(x_1) - \tfrac{\partial \mathrm{H}}{\partial x_3}(x_3) - z_2(w_2), \end{aligned} \tag{7}$$

with coil velocity $\mathrm{v_C} = \frac{\partial \mathrm{H}}{\partial x_2}(x_2) = \frac{\mathrm{d}x_3}{\mathrm{d}t} = w_2$ and current $i_C = \frac{\partial \mathrm{H}}{\partial x_2}(x_2) = w_1 = -y_1$. The corresponding structure is given in table 1.

Simulation results Simulations are performed following the passive-guaranteed numerical method associated with the pH structure (3) and recalled in appendix A. In practice, they are all produced by[1] the PyPHS python library. Results are shown in figure 4 for different values of the overhang parameter Q_ℓ. The symmetric relation assumed on $\ell_C(q_D)$ induces a doubling of the period in the force factor. Notice the (numerical) power balance is satisfied. The model 0 in table 1 is refined in the sequel to cope with the phenomena (1–7) listed in the introduction.

4 Refined mechanics

In this section, the model 0 from section 3.3 is refined to cope with creep effect and nonlinear stress-strain relation attached to the suspension material (S). First, we detail the modeling of the creep effect based on Kelvin-Voigt model of viscoelastic material **??**. This results in a linear PHS. Second, the hardening suspension effect is included. This results in a nonlinear PHS. This provides the model 1. Third, simulation results are shown.

4.1 Suspension creep

The creep effect is a long-term shape-memory of the suspension material: when a step force is applied,

[1]Simulation code are available here: `https://afalaize.github.io/posts/loudspeaker1/`

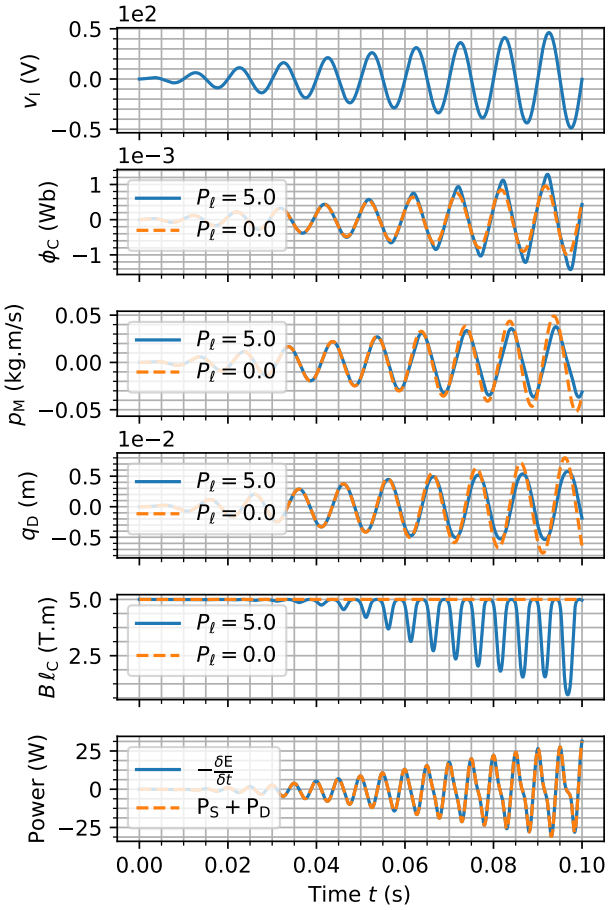

Figure 4: Simulation results for the model 0 in table 1. Physical parameters are given in table 6. The input voltage v_I is a 100Hz sine wave with increasing amplitude between 0 and 50V. The sampling rate is $F_s = 96$kHz. The power balance is shown for the case $P_\ell = 5$ only.

first the diaphragm moves quite instantaneously to an equilibrium for which the restoring force is exactly compensating, and second a very slow displacement occurs, due to rearrangements in the crystal lattice of the material (see *e.g.* [27, figure 1] and [37, figure 11]). This phenomenon is enhanced by heat relaxation of the fluid in the enclosure [51]: when the container is put under pressure, the fluid's pressure rise in an adiabatic process to compensate the external pressure, and then decreases with cooling due to exchanges with the anisothermal boundaries.

Several modeling of the creep effect have been proposed in the frequency domain, among which the *exp-model* (fractional differentiator) in [27, eq. (8)], the *log-model* (frequency-dependent stiffness) in [27], *FDD-model* (frequency-dependent damping) in [51, 50]. The frequency domain approach is motivated by the fact that long-time memory effects can be appropriately described by fractional-order linear dynamics (see *e.g.* [28, 19, 20], [39][part 6] and reference

therein for details). Here, we consider the standard Kelvin-Voigt model for viscoelastic materials. Its fractional extension proposed in [28] is postponed to a follow-up paper. The resulting (linear) mechanical subsystem is depicted in figure 5 and is recast in this subsection as a port-Hamiltonian system (3).

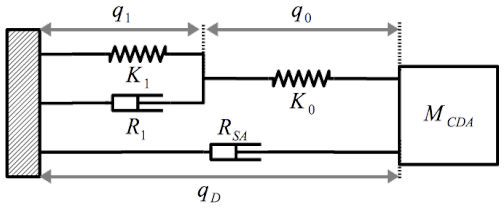

(a) Schematic of the considered mechanical subsystem.

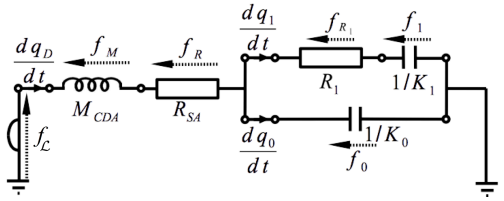

(b) Equivalent circuit.

Figure 5: Small-signal modeling of the mechanical part which includes: the total mass $M_{\texttt{CDA}}$ (diaphragm, coil and additional mass due to acoustic radiation), the fluid-like damper $R_{\texttt{SA}}$ (mechanical friction and small signal approximation for the acoustic power radiation), primary stiffness K_0 and Kelvin-Voigt modeling of the creep effect (K_1, R_1), with diaphragm position $q_{\texttt{D}}$, primary elongation q_0 and creep elongation q_1. Parameters are given in tables 6 and 7.

4.1.1 Description of the creep model

Viscoelastic materials exhibit combination of elastic solids behaviors and viscous fluid behaviors. Let R be the coefficient of viscosity for a damper ($\mathrm{N.s.m^{-1}}$) and K the modulus of elasticity for a spring element ($\mathrm{N.m^{-1}}$) with characteristic frequency $\omega = \frac{K}{R}$ (Hz) and associated *creep time* $\tau = \frac{2\pi}{\omega}$ (s). Their respective compliance in the Laplace domain are $\mathcal{T}_K = \frac{q(s)}{f_K(s)} = \frac{1}{K}$ and $\mathcal{T}_R = \frac{q(s)}{f_R(s)} = \frac{1}{R\,s}$ where s is the complex Laplace variable ($\Re e(s) > 0$) , and where $q(s)$, $f_K(s)$ and $f_R(s)$ are the Laplace transforms of the elongation and the two restoring forces, respectively.

The *Kelvin-Voigt* modeling of the creep effect is constructed by connecting a linear spring with same stiffness K in parallel with a damper r (see [2] and [28, § 4]). The elongation is the same for both elements $q_{\texttt{kv}} = q$ and forces sum up $f_{\texttt{kv}} = f_K + f_R$. The corresponding compliance is

$$\mathcal{T}_{\texttt{kv}}(s) = \frac{q_{\texttt{kv}}(s)}{f_{\texttt{kv}}(s)} = \left(K\,\left(1 + \frac{s}{\omega}\right)\right)^{-1}. \tag{8}$$

The modeling of materials that exhibits several relaxation times $\tau_n = \frac{2\pi}{\omega_n}$ is achieved by chaining N Kelvin-Voig elements (see [28, § 4], [33] and [2, figure 1]). Each element contributes to the total elongation $q_{\texttt{chain}} = \sum_{n=1}^{N} q_n$, and every elements experience the same force $f_{\texttt{chain}} = f_1 = \cdots = f_N$. The total compliance is therefore

$$\mathcal{T}_{\texttt{chain}}(s) = \frac{q_{\texttt{chain}}(s)}{f_{\texttt{chain}}(s)} = \sum_{n=1}^{N} \left(K_n\,\left(1 + \frac{s}{\omega_n}\right)\right)^{-1}, \tag{9}$$

with $\omega_n = \frac{K_n}{R_n}$. In this work, we consider three elements to restore (i) a primary instantaneous response to a step force with stiffness K_0 and (ii) a long time viscoelastic memory with characteristic time $\tau_{\texttt{ve}} = \frac{2\pi}{\omega_1}$. The compliance of this viscoelastic model is

$$\mathcal{T}_{\texttt{ve}}(s) = \frac{1}{K_0} + \left(K_1\,\left(1 + \frac{s}{\omega_1}\right)\right)^{-1}, \omega_1 = \frac{K_1}{R_1}. \tag{10}$$

We introduce the dimensionless parameter P_K to partition $K_{\texttt{SA}}$ between K_0 and K_1 so that $\mathcal{T}_{\texttt{ve}}(s)|_{\tau_{\texttt{ve}}=0} = K_{\texttt{SA}}/s$ for every value of $0 < P_K < 1$:

$$K_0 = \frac{K_{\texttt{SA}}}{1 - P_K}, \qquad K_1 = \frac{K_{\texttt{SA}}}{P_K}. \tag{11}$$

4.1.2 Port-Hamiltonian formulation

The creep model (10) corresponds to the parallel connection of (i) a linear spring K_0 and (ii) a linear spring K_1 serially connected to a dashpot R_1 (see figure 5). This mechanical subsystem includes $n_{\mathbf{x}} = 3$ storage components (mass $M_{\texttt{CDA}}$, primary stiffness K_0, secondary stiffness K_1), $n_{\mathbf{w}} = 2$ dissipative components (damper $R_{\texttt{SA}}$, secondary damper R_1), and $n_{\mathbf{y}} = 1$ port (Lorentz force $f_{\mathcal{L}}$). The state $\mathbf{x} = (p_{\texttt{M}}, q_0, q_1)^{\intercal}$ includes the mass momentum $p_{\texttt{M}} = M_{\texttt{CDA}}\,q_{\texttt{D}}$, and the primary and secondary elongations q_0 and q_1 (respectively). The Hamiltonian is the sum of (i) the kinetic energy $\mathrm{H}_{\texttt{M}}(x_1) = \frac{x_1^2}{2M_{\texttt{CDA}}}$, and (ii) the primary and secondary potential energies $\mathrm{H}_0(x_2) = K_0\frac{x_2^2}{2}$ and $\mathrm{H}_1(x_3) = K_1\frac{x_3^2}{2}$ (respectively). The dissipation variable is $\mathbf{w} = \left(\frac{\mathrm{d}q_{\texttt{D}}}{\mathrm{d}t}, f_{R_1}\right)^{\intercal}$ with linear dissipation law $\mathbf{z}(\mathbf{w}) = \mathrm{diag}(R_{\texttt{SA}}, R_1^{-1}) \cdot \mathbf{w}$. The input/output are $\mathbf{u} = (f_{\mathcal{L}})^{\intercal}$ and $\mathbf{y} = \left(\frac{\mathrm{d}q_{\texttt{D}}}{\mathrm{d}t}\right)^{\intercal}$. For these definitions, the interconnection in figure 5 yields

$$\begin{array}{rcl} \frac{\mathrm{d}x_1}{\mathrm{d}t} & = & -\frac{\partial \mathrm{H}}{\partial x_2}(x_2) - z_1(w_1) + u_1, \\ \frac{\mathrm{d}x_2}{\mathrm{d}t} & = & \frac{\partial \mathrm{H}}{\partial x_1}(x_1) - z_2(w_2), \\ \frac{\mathrm{d}x_3}{\mathrm{d}t} & = & z_2(w_2). \end{array} \tag{12}$$

This system is recast as a port-Hamiltonian system (3) for the structure in table 2 and the parameters in table 7.

4.2 Suspension hardening and model 1

For large displacement, the suspension behaves like an hardening spring (see phenomenon 5 and [1, 15]).

Storage

State: $\mathbf{x} = (p_{\mathtt{M}}, q_0, q_1)^\intercal$ — Energy: $\mathrm{H}(\mathbf{x}) = \mathbf{x}^\intercal\,\mathbf{Q}\,\mathbf{x}$

Dissipation

Variable: $\mathbf{w} = \left(\frac{\mathrm{d}q_{\mathtt{D}}}{\mathrm{d}t}, f_{R_1}\right)^\intercal$ — Law: $\mathbf{z}(\mathbf{w}) = \mathbf{R}\,\mathbf{w}$

Ports

Input: $\mathbf{u} = (f_{\mathcal{L}})^\intercal$ — Output: $\mathbf{y} = \left(\frac{\mathrm{d}q_{\mathtt{D}}}{\mathrm{d}t}\right)^\intercal$

Structure

$$\mathbf{J}_{\mathbf{x}} = \begin{pmatrix} 0 & -1 & 0 \\ 1 & 0 & 0 \\ 0 & 0 & 0 \end{pmatrix}, \mathbf{K} = \begin{pmatrix} 1 & 0 \\ 0 & 1 \\ 0 & -1 \end{pmatrix},$$

$$\mathbf{G}_{\mathbf{x}} = \left(1, 0, 0\right)^\intercal, \mathbf{J}_{\mathbf{w}} = \mathbb{0}, \mathbf{G}_{\mathbf{w}} = \mathbb{0}, \mathbf{J}_{\mathbf{y}} = 0.$$

Table 2: Port-Hamiltonian formulation (3) for the proposed small signal model of the mechanical part in figure 5 driven by the Lorentz force $f_{\mathcal{L}}$, with diaphragm position $q_{\mathtt{D}}$, momentum $p_M = M_{\mathtt{CDA}}\frac{\mathrm{d}q_{\mathtt{D}}}{\mathrm{d}t}$, primary elongation q_0, and creep elongation q_1. Parameters are given in tables 6 and 7, with $\mathbf{Q} = \frac{1}{2}\mathrm{diag}(\frac{1}{M_{\mathtt{CDA}}}, K_0, K_1)$ and $\mathbf{R} = \mathrm{diag}(R_{\mathtt{SA}}, R_1^{-1})$.

This should occur for instantaneous displacements, so that only the primary stiffness K_0 in table 2 is affected. First, the mechanical subsystem from previous section is changed to cope with this phenomenon. Second, the resulting nonlinear mechanical part is included in loudspeaker model 0 to build the loudspeaker model 1.

4.2.1 Model description

The primary stiffness K_0 in table 2 is modified into a nonlinear spring that exhibits a phenomenological saturation for an instantaneous elongation $q_0 = \pm q_{\mathtt{sat}}$ (symmetric). The associated constitutive law (38–40) in appendix C is

$$c_{\mathtt{SA}}(q_0) = q_0 + \frac{4\,P^{\mathtt{S}}_{\mathtt{sat}}}{4-\pi}\left(\tan\left(\frac{\pi.q_0}{2\,q_{\mathtt{sat}}}\right) - \frac{\pi.q_0}{2q_{\mathtt{sat}}}\right). \quad (13)$$

It yields the restoring force $f_0(q_0) = K_0\,c_{\mathtt{SA}}(q_0)$ for the initial stiffness K_0. It corresponds to the addition of a saturating term that does not contribute around the origin, thus preserving the meaning of parameter K_0 (small signal behavior). The associated storage function (41–42) is

$$\mathrm{H}^{\mathtt{SA}}_{\mathtt{sat}}(q_0) = K_0\left(\frac{q_0^2}{2} - \frac{8P^{\mathtt{S}}_{\mathtt{sat}}\,q_{\mathtt{sat}}}{\pi(4-\pi)}\left(\ln\left|\cos\left(\frac{\pi\,q_0}{2\,q_{\mathtt{sat}}}\right)\right| + \frac{1}{2}\left(\frac{\pi\,q_0}{2q_{\mathtt{sat}}}\right)^2\right)\right) \geq 0. \quad (14)$$

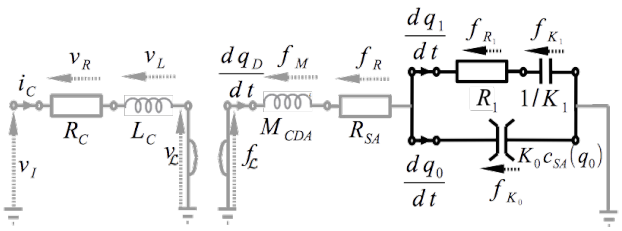

Figure 6: Equivalent circuit for model 1 with diaphragm position $q_{\mathtt{D}}$, primary elongation q_0 and creep elongation q_1. Elements common to model 0 in figure 2 are shaded.

4.2.2 Port-Hamiltonian system and Model 1

The port-Hamiltonian formulation of the loudspeaker model 1 includes creep effect (phenomenon 4) and hardening suspension (phenomenon 5). It is obtained by (i) replacing the potential energy $K_0\frac{q_0^2}{2}$ in table 2 by the nonlinear storage function (14) and (ii) connecting the mechanical port $f_{\mathcal{L}}$ to the RL circuit describing the electromagnetic part as in section **??**. This results in the structure given in table 3 with parameters in tables 6 and 7.

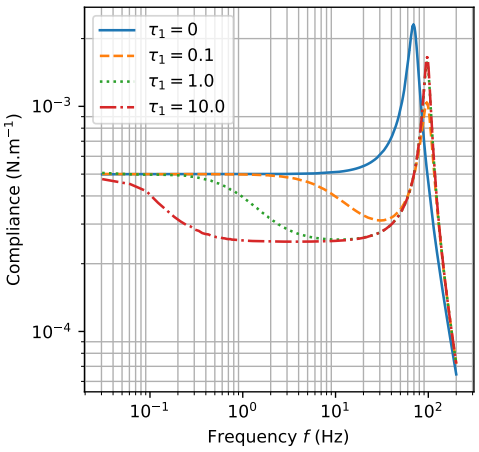

Figure 7: Simulation of the small-signal modeling of the mechanical subsystem in table 2: Compliance in the frequency domain (diaphragm displacement in response to the Lorentz force $\left|\frac{q_{\mathtt{D}}}{f_{\mathcal{L}}}\right|(2i\pi f)$). The low-frequency effect is clearly visible.

Storage

State: $\mathbf{x} = (\phi_{\mathtt{C}}, p_{\mathtt{M}}, q_0, q_1)^\intercal$

Energy: $\mathrm{H}(\mathbf{x}) = \mathbf{x}^\intercal\,\mathbf{Q}\,\mathbf{x} + \mathrm{H}^{\mathtt{SA}}_{\mathtt{sat}}(x_3)$

Dissipation

Variable: $\mathbf{w} = \left(i_{\mathtt{C}}, \frac{\mathrm{d}q_{\mathtt{D}}}{\mathrm{d}t}, f_{R_1}\right)^\intercal$

Law: $\mathbf{z}(\mathbf{w}) = \mathbf{R}\,\mathbf{w}$

Ports

Input: $\mathbf{u} = (v_{\mathtt{I}})^\intercal$

Output: $\mathbf{y} = (-i_{\mathtt{C}})^\intercal$

Structure

$$\mathbf{J}_{\mathbf{x}} = \begin{pmatrix} 0 & -B\ell_{\mathtt{C}}(q_{\mathtt{D}}) & 0 & 0 \\ B\ell_{\mathtt{C}}(q_{\mathtt{D}}) & 0 & -1 & 0 \\ 0 & 1 & 0 & 0 \\ 0 & 0 & 0 & 0 \end{pmatrix},\ \mathbf{G}_{\mathbf{x}} = \begin{pmatrix} 1 \\ 0 \\ 0 \\ 0 \end{pmatrix},$$

$$\mathbf{K} = \begin{pmatrix} 1 & 0 & 0 \\ 0 & 1 & 0 \\ 0 & 0 & -1 \\ 0 & 0 & 1 \end{pmatrix},\ \mathbf{J}_{\mathbf{w}} = \mathbb{0},\ \mathbf{G}_{\mathbf{w}} = \mathbb{0},\ \mathbf{J}_{\mathbf{y}} = 0.$$

Table 3: Port-Hamiltonian formulation (3) for the model 1 depicted in figure 9. The linear stiffness $K_{\mathtt{SA}}$ is replaced by the Kelvin-Voigt modeling of the creep effect from section 4.1 in serial connection with the nonlinear spring described in section4.2, with diaphragm position $q_{\mathtt{D}}$, momentum $p_M = M_{\mathtt{CDA}}\frac{\mathrm{d}q_{\mathtt{D}}}{\mathrm{d}t}$, primary elongation q_0, and creep elongation q_1. The nonlinear potential energy $\mathrm{H}^{\mathtt{SA}}_{\mathtt{sat}}(q_0)$ is given in (14). Parameters are given in tables 6 and 7, with $\mathbf{Q} = \frac{1}{2}\mathrm{diag}(\frac{1}{L_{\mathtt{C}}}, \frac{1}{M_{\mathtt{CDA}}}, K_0, K_1,)$ and $\mathbf{R} = \mathrm{diag}(R_{\mathtt{C}}, R_{\mathtt{SA}}, R_1)$.

4.3 Simulation results

The numerical method used to simulate model 1 is detailed in appendix A. The results obtained for physical parameters in table 6 and 7 are commented below.

Creep effect (Phenomenon 4) It is expected that the viscoelastic behavior of the suspension material results in a frequency-dependent compliance, *i.e.* the suspension at low frequencies must appear softer than for the Thiele/Small prediction (see *e.g.* [51, figure 12]). Model 1 allows the recovery of this effect as shown in figures 7. The corresponding long time memory depicted in figures 8 is in accordance with measurements in *e.g.* [27, figure 1] and [37, figure 11].

Nonlinear suspension (Phenomenon 5) The hardening effect associated with the nonlinear stress–strain characteristic of the suspension material is clearly visible in figure 9 where the primary elongation is reduced for higher value of the shape parameter $P^{\mathtt{S}}_{\mathtt{sat}}$. This reduces the total displacement $q_{\mathtt{D}}$ and momentum $p_{\mathtt{M}} = M_{\mathtt{CDA}}\frac{\mathrm{d}q_{\mathtt{D}}}{\mathrm{d}t}$, while the creep elongation is almost unchanged. Notice in the last sub-figure that the power balanced is fulfilled with $\frac{\mathrm{dE}}{\mathrm{d}t} = \mathrm{P_S} - \mathrm{P_D}$.

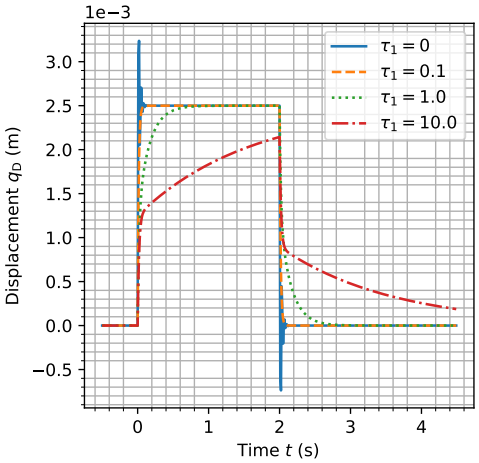

Figure 8: Simulation of the small-signal modeling of the mechanical subsystem in table 2: diaphragm displacement in response to a 10N Lorentz force step between 0s and 2s (time domain).

5 Refined electromagnetic

In this section, the model 0 from section 3.3 is refined to account for effects of flux modulation (phenomenon 2), electromagnetic coupling (phenomenon 3), ferromagnetic saturation (phenomenon 6) and eddy-current losses (phenomenon 7) attached to the electromagnetic part (voice-coil `C`, magnet `M`, ferromagnetic path `P` and air gap `G`). First, the proposed modeling is described. Second, this model is recast as a port-Hamiltonian system. Third, simulation results are presented.

5.1 Model description

The classical lumped elements modeling of loudspeakers electrical impedance includes the electrical DC resistance of the wire $R_{\mathtt{C}}$ serially connected to a non-standard inductive effect, referred as *lossy-inductor*. The simplest refinement of the Thiele/Small modeling is the so-called *LR-2 model*, which uses a series inductor connected to a second inductor shunted by a resistor. This structure has been refined by several authors [53, 54, 11, 52, 29] by considering nonstandard components instead of the ideal resistances and inductances to recover the measured electrical impedance. For instance, a frequency-dependent inductance has

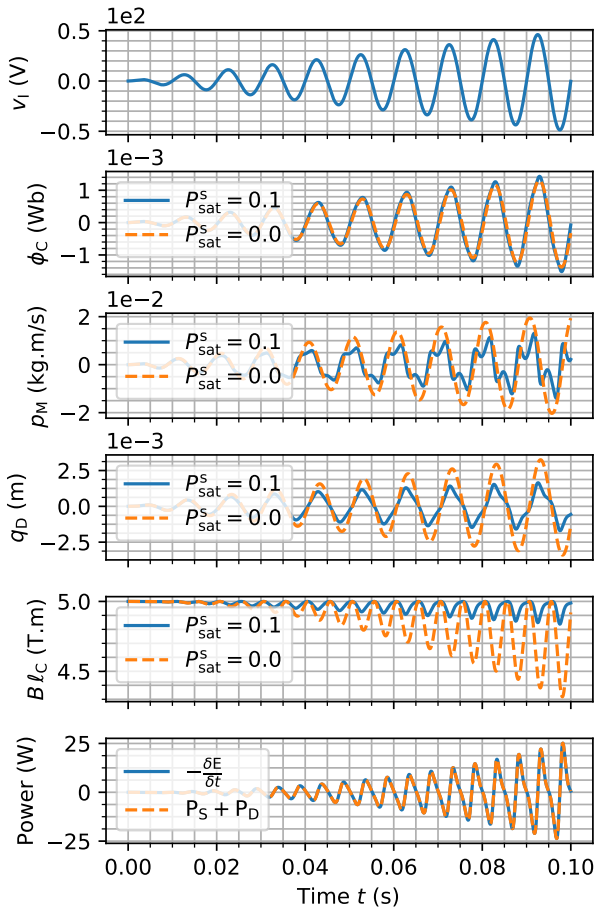

Figure 9: Simulation of the model 1 in table 3 depicted in figure 9, for the parameters in tables 6 and 7 (except $P^{\mathtt{S}}_{\mathtt{sat}}$ indicated in the legend). The input voltage is a 100Hz sine wave with increasing amplitude between 0V and 50V. The sampling rate $f_s = 96$kHz. The power balance is shown for $P^{\mathtt{S}}_{\mathtt{sat}} = 10$ only. Notice $q_{\mathtt{D}} = q_0 + q_1$.

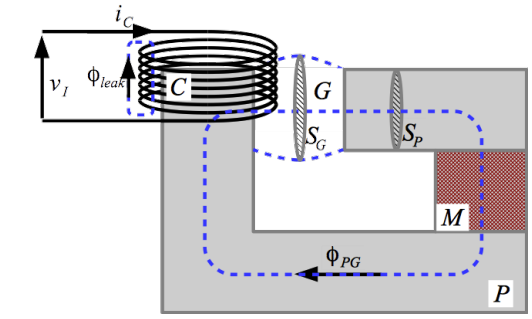

(a) Schematic

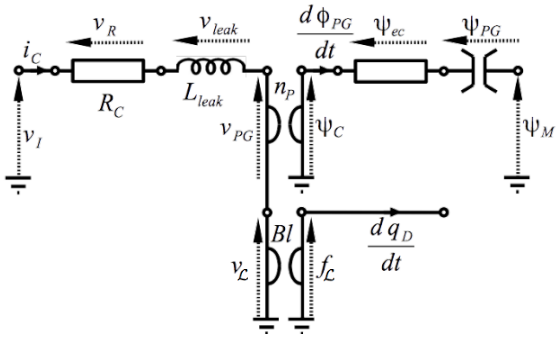

(b) Equivalent circuit

Figure 10: Proposed modeling of the electromagnetic circuit, which includes: the coil wire resistance $R_{\mathtt{C}}$, the linear inductance associated with the leakage flux $\phi_{\mathtt{leak}}$, the electromagnetic transduction with $n_{\mathtt{P}}$ the number of wire turns around the magnetic path, the magnetic energy storage in the ferromagnetic path described by the nonlinear induction–excitation curve $\psi_{\mathtt{PG}}(\phi_{\mathtt{PG}})$ from (18), the linear dissipation associated with eddy-currents in the pole piece, and the constant source of magnetomotive force $\psi_{\mathtt{M}}$ due to the magnet from (20).

been considered in [53], and a weighted power function of the frequency for both the real and imaginary part of the impedance has been proposed in [54, 32].

Here, the proposed modeling of the loudspeakers electrical impedance is depicted in figure 10. The coil winding acts as an electromagnetic transducer (gyrator) that realizes a coupling between the electrical and the magnetic domains, according to the gyrator-capacitor approach (see appendix B.3 and [9, 18]). The electrical domain includes the linear resistance $R_{\mathtt{C}}$ of the coil wire (same as Thiele-Small model) and a constant linear inductance associated with the leakage magnetic flux that does not penetrate the pole piece (P). The flux in the magnetic path is common to (i) a nonlinear magnetic capacitor associated with energy storage in air gap (G, linear) and ferromagnetic (P, nonlinear), (ii) a linear magnetic dissipation associated with eddy-currents losses in the path (P) and (iii) a constant source of magnetomotive force associated with the permanent magnet (Ampère model).

5.1.1 Coil model

Leakage inductance A single leakage flux $\phi_{\mathtt{leak}} = S_{\mathtt{leak}}\, b_{\mathtt{leak}}$ independent of the position $q_{\mathtt{D}}$ is assumed for every of the $N_{\mathtt{C}}$ wire turns (see 10a), with $S_{\mathtt{leak}}$ the annular surface between the coil winding and the ferromagnetic core, computed as

$$S_{\mathtt{leak}} = \frac{\pi\, D_{\mathtt{C}}^2}{4}\,(2\,\alpha_{\mathtt{leak}} - \alpha_{\mathtt{leak}}^2), \qquad (15)$$

where $0 < \alpha_{\mathtt{leak}} < 1$ is the fraction of the coil section not occupied by the magnetic core. According to (33), the linear magnetic capacity of the air path is $C_{\mathtt{leak}} = \frac{S_{\mathtt{leak}}\,\mu_0\,(1+\xi_{\mathtt{air}})}{2\,A_{\mathtt{C}}}$ with $A_{\mathtt{C}}$ the height of the coil wire turns, μ_0 the magnetic permeability of vacuum and $\xi_{\mathtt{air}}$ the magnetic susceptibility of air. From (37), this corresponds to an electrical inductance with state $x_{\mathtt{leak}} = N_{\mathtt{C}}\,\phi_{\mathtt{leak}}$ and storage function $\mathrm{H}_{\mathtt{leak}}(x_{\mathtt{leak}}) = \frac{{x_{\mathtt{leak}}}^2}{2L_{\mathtt{leak}}}$, for the inductance

$L_{\mathtt{leak}} = N_{\mathtt{C}}^2\, C_{\mathtt{leak}}$. We define the characteristic frequency $\omega_{\mathtt{C}} = \frac{R_{\mathtt{C}}}{L_{\mathtt{leak}}}$ (Hz).

Electromagnetic coupling modulation The electromagnetic coupling between the coil (C) and the path (P) depends on the he number $n_{\mathtt{P}}$ of wire turns effectively surrounding the pole piece. For small negative excursions $q_{\mathtt{D}} < 0$ every *wire turns* participate to the coupling ($n_{\mathtt{P}} \simeq N_{\mathtt{C}}$) and for large positive excursions the coil leaves the pole piece ($n_{\mathtt{P}} \simeq 0$). We propose a phenomenological sigmoid relation $n_{\mathtt{P}} : q_{\mathtt{D}} \mapsto n_{\mathtt{P}}(q_{\mathtt{D}})$:

$$n_{\mathtt{P}}(q_{\mathtt{D}}) = N_{\mathtt{C}} \left(1 + \exp\left(\frac{4\,q_{\mathtt{D}} - 2\,(q_- + q_+)}{q_+ - q_-}\right)\right)^{-1}, \tag{16}$$

with $n_{\mathtt{P}}(q_-) \simeq 90\% N_{\mathtt{C}}$ and $n_{\mathtt{P}}(q_+) \simeq 10\% N_{\mathtt{C}}$ (see figure 11).

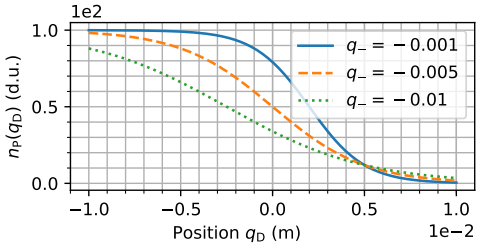

Figure 11: Plot of the position-dependent effective number of wire turns $n_{\mathtt{P}}(q_{\mathtt{D}})$ involved in the electromagnetic coupling from (16) with $q_+ = 5$mm and q_- in the legend.

5.1.2 Ferromagnetic saturation

Nonlinear storage The storage of magnetic energy in the magnetic circuit is spread over the pole piece (P) and the air gap (G). Assuming no leakage flux in the pole piece, those elements are crossed by the same magnetic flux $\phi_{\mathtt{PG}}$ (see figure 10a and [9, 18]). The corresponding averaged inductions are

$$\begin{aligned} b_{\mathtt{P}} &= \tfrac{\phi_{\mathtt{PG}}}{S_{\mathtt{P}}}, \\ b_{\mathtt{G}} &= \tfrac{\phi_{\mathtt{PG}}}{S_{\mathtt{G}}}, \end{aligned} \tag{17}$$

with $S_{\mathtt{P}}$ the average section crossed by the magnetic flux in the pole piece and $S_{\mathtt{G}}$ the section of the flux in the air gap (see figure 10a). This corresponds to the serial connection of two magnetic capacitors: the first one is associated with the air gap G with linear constitutive law (as for the leakage flux $\phi_{\mathtt{leak}}$); the second one is associated with the pole piece P and cannot be described by a linear magnetic capacity due to the magnetic saturation that occurs in ferromagnetic material (phenomenon 6, see also [17, §1]). Those two serially-connected magnetic capacitors can merge into a single nonlinear capacitor that restores the total magnetomotive force $\psi_{\mathtt{PG}}(\phi_{\mathtt{PG}})$. We consider the tangent-like constitutive relation detailed in appendix C with flux saturation $\phi_{\mathtt{sat}} = S_{\mathtt{P}}\, b_{\mathtt{sat}}$, where $b_{\mathtt{sat}}$ depends on the specific magnetic material. From (38–40), the constitutive law $\psi_{\mathtt{PG}}(\phi_{\mathtt{PG}}) = c_{\mathtt{PG}}(\phi_{\mathtt{PG}})$ is given by

$$c_{\mathtt{PG}}(\phi_{\mathtt{PG}}) = P_{\mathtt{lin}}^{\mathtt{PG}} \left(\phi_{\mathtt{PG}} + \tfrac{4\,P_{\mathtt{sat}}^{\mathtt{PG}}}{4-\pi} \left(\tan\left(\tfrac{\pi\,\phi_{\mathtt{PG}}}{2\,\phi_{\mathtt{sat}}}\right) - \tfrac{\pi\,\phi_{\mathtt{PG}}}{2\phi_{\mathtt{sat}}}\right)\right), \tag{18}$$

where the coefficient $P_{\mathtt{lin}}^{\mathtt{PG}}$ includes the contributions of both air and pole piece material, and $P_{\mathtt{sat}}^{\mathtt{PG}}$ is a function shape parameter that depends on the specific material used for the pole piece. The associated (semi-positive definite) storage function (41–42) is given by

$$\begin{aligned} &\mathrm{H}_{\mathtt{sat}}^{\mathtt{PG}}(\phi_{\mathtt{PG}}) = \\ &P_{\mathtt{lin}}^{\mathtt{PG}} \left(\tfrac{\phi_{\mathtt{PG}}^2}{2} - \tfrac{8 P_{\mathtt{sat}}^{\mathtt{PG}}\,\phi_{\mathtt{sat}}}{\pi(4-\pi)} \left(\ln\left|\cos\left(\tfrac{\pi\,\phi_{\mathtt{PG}}}{2\,\phi_{\mathtt{sat}}}\right)\right| + \tfrac{1}{2}\left(\tfrac{\pi\,\phi_{\mathtt{PG}}}{2\phi_{\mathtt{sat}}}\right)^2\right)\right). \end{aligned} \tag{19}$$

Steady state behavior The permanent magnet is modeled as a constant source of magnetomotive force $\psi_{\mathtt{M}}$ (Ampère model [18]). This drives the magnetic flux in the path to an equilibrium (steady-state ss) $\phi_{\mathtt{PG}} = \phi_{\mathtt{ss}}$ for which the magnetomotive force exactly compensates that of the magnet:

$$\psi_{\mathtt{PG}}(\phi_{\mathtt{ss}}) = -\psi_{\mathtt{M}}. \tag{20}$$

The associated steady-state magnetic capacity is the inverse of the linear approximation of $\psi_{\mathtt{PG}}(\phi_{\mathtt{PG}})$ at $\phi_{\mathtt{ss}}$:

$$C_{\mathtt{ss}} = \left(\left.\frac{\partial c_{\mathtt{PG}}}{\partial \phi_{\mathtt{PG}}}\right|_{\phi_{\mathtt{PG}}=\phi_{\mathtt{ss}}}\right)^{-1} = \left(\left.\frac{\partial^2 \mathrm{H}_{\mathtt{sat}}^{\mathtt{PG}}}{\partial \phi_{\mathtt{PG}}^2}\right|_{\phi_{\mathtt{PG}}=\phi_{\mathtt{ss}}}\right)^{-1}, \tag{21}$$

with

$$\tfrac{\partial^2 \mathrm{H}_{\mathtt{sat}}^{\mathtt{PG}}}{\partial \phi_{\mathtt{PG}}^2}(\phi_{\mathtt{PG}}) = P_{\mathtt{lin}}^{\mathtt{PG}} \left(1 + \tfrac{2\pi P_{\mathtt{sat}}^{\mathtt{PG}}}{(\pi-4)\phi_{\mathtt{sat}}} \left(1 - \cos^{-2}\left(\tfrac{\pi\phi_{\mathtt{PG}}}{2\phi_{\mathtt{sat}}}\right)\right)\right),$$

so that $P_{\mathtt{lin}}^{\mathtt{PG}}$ can be tuned according to

$$P_{\mathtt{lin}}^{\mathtt{PG}} = \frac{(\pi-4)\phi_{\mathtt{sat}}}{C_{\mathtt{ss}}\left(2\pi P_{\mathtt{sat}}^{\mathtt{PG}}\left(1-\cos^{-2}\left(\frac{\pi\phi_{\mathtt{ss}}}{2\phi_{\mathtt{sat}}}\right)\right)+(\pi-4)\phi_{\mathtt{sat}}\right)}, \tag{22}$$

with $C_{\mathtt{ss}} = \frac{L_{\mathtt{P}}}{n_{\mathtt{P}}(0)^2}$ and $L_{\mathtt{P}} = L_{\mathtt{C}} - L_{\mathtt{leak}}$.

5.1.3 Eddy-currents losses

Besides the magnetic saturation, the pole piece is affected by the combination of capacitive and resitive effects due to eddy-currents, resulting in frequency-dependent losses (phenomenon 7). This phenomenon is well described by a linear fractional order magnetic capacity (see [31, 39, 40, 38, 8, 6] and [39][part 5]). This is out the scope of the present work and is postponed to a follow-up paper. Here, we consider a magnetic resistance $R_{\mathtt{ec}}$ (Ω^{-1}) with magnetic impedance

$$\mathcal{T}_{\mathtt{ec}}(s) = \frac{\psi_{\mathtt{ec}}(s)}{s\,\phi_{\mathtt{ec}}(s)} = R_{\mathtt{ec}}. \tag{23}$$

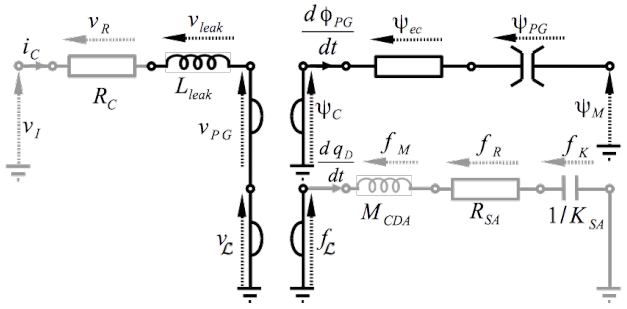

Figure 12: Equivalent circuit of the model 2 described in table 4. Elements common to model 0 in figure 2 are shaded. The coil inductance $L_{\mathtt{C}}$ is replaced by the electromagnetic circuit from figure 10b which includes the leakage inductance $L_{\mathtt{leak}}$ and the magnetic path (pole piece P and air gap G).

Since we consider a single magnetic flux in the pole piece $\phi_{\mathtt{ec}} = \phi_{\mathtt{PG}}$, this impedance is serially connected to the magnetic capacity described in 5.1.2. The resulting structure is depicted in figure 10b. Defining $\omega_{\mathtt{P}} = (R_{\mathtt{ec}}\, C_{\mathtt{ss}})^{-1}$ (Hz) and $\tau_{\mathtt{P}} = \frac{2\pi}{\omega_{\mathtt{P}}}$ (s), the resulting electrical impedance $\mathcal{T}_{\mathtt{P}}(s) = \frac{v_{\mathtt{P}}}{i_{\mathtt{C}}}$ is

$$\mathcal{T}_{\mathtt{P}}(s) = \frac{v_{\mathtt{P}}(s)}{i_{\mathtt{C}}(s)} = \frac{n_{\mathtt{P}}(q_{\mathtt{D}})^2}{R_{\mathtt{ec}}}\,\frac{s}{s+\omega_{\mathtt{P}}}. \tag{24}$$

5.1.4 Blocked electrical impedance

The current $i_{\mathtt{C}}$ is common to (i) the resistor $R_{\mathtt{C}}$, (ii) the leakage inductance $L_{\mathtt{leak}}$, and (iii) the impedance associated with the magnetic path in the coil core $\mathcal{T}_{\mathtt{P}}(s)$. For a blocked coil ($\frac{\mathrm{d}q_{\mathtt{D}}}{\mathrm{d}t} = 0 \Rightarrow v_{\mathcal{L}} = 0$), the total steady-state electrical impedance $\mathcal{T}_{\mathtt{C}}(s) = \frac{v_{\mathtt{I}}(s)}{i_{\mathtt{C}}(s)}$ measured at the coil terminals is given by

$$\mathcal{T}_{\mathtt{C}}(s) = R_{\mathtt{C}}\left(1 + \frac{s}{\omega_{\mathtt{C}}}\left(1 + \frac{n_{\mathtt{P}}(q_{\mathtt{D}})^2}{R_{\mathtt{C}}R_{\mathtt{ec}}}\,\frac{\omega_{\mathtt{C}}}{s+\omega_{\mathtt{P}}(\phi_{\mathtt{PG}})}\right)\right). \tag{25}$$

The DC value ($s = 0$) is given by the resistance $R_{\mathtt{C}}$. In the high frequency range, the impedance is governed by the leakage inductance $\mathcal{T}_{\mathtt{C}}(i\,\omega) \underset{\omega\to\infty}{\sim} R_{\mathtt{C}}\left(1 + \frac{i\,\omega}{\omega_{\mathtt{C}}}\right)$. The inner bracket is the contribution of the proposed magnetic circuit.

5.2 Port-Hamiltonian formulation

The proposed loudspeaker modeling that includes electromagnetic phenomena (model 2) corresponds to the replacement of the inductance $L_{\mathtt{C}}$ in model 0 by the electromagnetic circuit described in previous section (compare figures 2 and 12). It includes (i) the resistance-inductance circuit $R_{\mathtt{C}}$–$L_{\mathtt{leak}}$ serially connected to (ii) the magnetic circuit associated with the core of the coil and the magnet. This involves $n_{\mathbf{x}} = 4$ storage components (inductance $L_{\mathtt{leak}}$, capacity $c_{\mathtt{PG}}$, mass $M_{\mathtt{CDA}}$, and stiffness $K_{\mathtt{SA}}$), $n_{\mathbf{w}} = 3$ dissipative components (resistances $R_{\mathtt{C}}$, $R_{\mathtt{SA}}$ and $R_{\mathtt{ec}}$), and $n_{\mathbf{y}} = 2$ ports (voltage $v_{\mathtt{I}}$ and magnetomotive force $\psi_{\mathtt{M}}$). The state is $\mathbf{x} = (x_{\mathtt{leak}}, \phi_{\mathtt{PG}}, p_{\mathtt{M}}, q_{\mathtt{D}})^{\intercal}$ with stae associated with leakage flux $x_{\mathtt{leak}} = N_{\mathtt{C}}\,\phi_{\mathtt{leak}}$, and the Hamiltonian is $\mathrm{H}(\mathbf{x}) = \mathbf{x}^{\intercal}\mathbf{Q}\mathbf{x} + \mathrm{H}^{\mathtt{PG}}_{\mathtt{sat}}(x_2)$ with $\mathbf{Q} = \frac{1}{2}\mathrm{diag}(\frac{1}{L_{\mathtt{leak}}}, 0, \frac{1}{M_{\mathtt{CDA}}}, K_{\mathtt{SA}})$ and $\mathrm{H}^{\mathtt{PG}}_{\mathtt{sat}}$ given in (19). The dissipation variable is $\mathbf{w} = (i_{\mathtt{C}}, \frac{\mathrm{d}q_{\mathtt{D}}}{\mathrm{d}t}, \psi_{\mathtt{PG}})^{\intercal}$ with linear dissipation law $\mathbf{z}(\mathbf{w}) = \mathrm{diag}(R_{\mathtt{C}}, R_{\mathtt{SA}}, {R_{\mathtt{ec}}}^{-1})\,\mathbf{w}$. According to (17), the magnetic induction in the air gap involved in the electromechanical coupling (35) is $b_{\mathtt{G}} = \frac{\phi_{\mathtt{PG}}}{S_{\mathtt{G}}}$. The length of wire effectively subjected to the induction field is $\ell_{\mathtt{C}}(x_4)$ given in (6). The number of wire turns effectively surrounding the pole piece involved in the electromagnetic coupling is $n_{\mathtt{P}}(x_4)$ given in (16). With these definitions, the port-Hamiltonian formulation (3) of the loudspeaker model with the refined electromagnetic part (model 2 depicted in figure 10) is given in table 4.

5.3 Simulation results

The numerical method used to simulate model 2 is still that detailed in appendix A. Physical parameters are given in table 6 and 8. In each case, the initial condition is the steady-state $\phi_{\mathtt{PG}}(t=0) = x_2(t=0) = \phi_{\mathtt{ss}}$.

Eddy-current losses (phenomenon 7) The effect of the characteristic time $\tau_{\mathtt{ec}} = 2\pi R_{\mathtt{ec}} C_{\mathtt{ss}}$ due to eddy-currents in the pole piece is illustrated by imposing several DC input voltages $v_{\mathtt{I}}$, here -50V, 0V and 50V (see evolution of flux $\phi_{\mathtt{PG}}$ in figure 13), with the coil blocked at $q_{\mathtt{D}} = 0$m and $C_{\mathtt{ss}}$ kept fixed, so that only $R_{\mathtt{ec}}$ varies with $\tau_{\mathtt{ec}}$. In each case, the magnetic flux in the path is driven to a new steady state $\phi_{\mathtt{PG}} \neq \phi_{\mathtt{ss}}$. The long-term effects and the influence of the characteristic time $\tau_{\mathtt{PG}}$ are clearly visible.

Core saturation (phenomenon 6) The evolution of the small signal impedance with the steady-state is shown in figure 14. First, the DC input voltages are imposed during 0.5 s. Second, a small signal noise is applied to evaluate the new steady-state blocked-impedance. We see an evolution in the high-frequency response according to the transfer function in (25). The associated value for is given in $C_{\mathtt{ss}}$ from (21) and the other parameters are given in table 8.

Position-dependent electromagnetic coupling (phenomenon 3) To illustrate the effect of coil position on the electrical impedance, position $q_{\mathtt{D}}$ in model 2 (table 4) is fixed to -1cm (inside), 0cm (equilibrium) and +1cm (outside). Due to the position-dependent effective number of coil wire (16), this changes the inductance according to (37). Results are shown in figure 15, in accordance with measurements in *e.g.* [26, figure 6].

Storage

State: $\mathbf{x} = \begin{pmatrix} x_{\mathtt{leak}} \\ \phi_{\mathtt{PG}} \\ p_{\mathtt{M}} \\ q_{\mathtt{D}} \end{pmatrix}$

Energy: $\mathrm{H}(\mathbf{x}) = \mathbf{x}^\intercal \mathbf{Q}\, \mathbf{x} + \mathrm{H}^{\mathtt{PG}}_{\mathtt{sat}}(x_2)$

Dissipation

Variable: $\mathbf{w} = (i_{\mathtt{C}}, \frac{\mathrm{d}q_{\mathtt{D}}}{\mathrm{d}t}, \psi_{\mathtt{PG}})^\intercal$

Law: $\mathbf{z}(\mathbf{w}) = \mathbf{R}\,\mathbf{w}$

Ports

Input: $\mathbf{u} = (v_{\mathtt{I}}, \psi_{\mathtt{M}})^\intercal$

Output: $\mathbf{y} = (-i_{\mathtt{C}}, \frac{\mathrm{d}\phi_{\mathtt{PG}}}{\mathrm{d}t})^\intercal$

Structure

$$\mathbf{J}_{\mathbf{x}} = \begin{pmatrix} 0 & 0 & -B_\ell(\mathbf{x}) & 0 \\ 0 & 0 & 0 & 0 \\ B_\ell(\mathbf{x}) & 0 & 0 & -1 \\ 0 & 0 & 1 & 0 \end{pmatrix},$$

$$\mathbf{G}_{\mathbf{x}} = \begin{pmatrix} 1 & 0 \\ 0 & 0 \\ 0 & 0 \\ 0 & 0 \\ \mathbb{0} & \mathbb{0} \end{pmatrix}, \mathbf{K} = \begin{pmatrix} 1 & 0 & n_{\mathtt{P}}(\mathbf{x}) \\ 0 & 0 & -1 \\ 0 & 1 & 0 \\ 0 & 0 & 0 \end{pmatrix},$$

$$\mathbf{G}_{\mathbf{w}} = \begin{pmatrix} 0 & 0 \\ 0 & 0 \\ 0 & -1 \end{pmatrix},$$

Table 4: Blocks associated with the port-Hamiltonian formulation (3) for the loudspeaker model 2 depicted in figure 10, where the Lorentz force factor is $B_\ell(\mathbf{x}) = \frac{x_2}{S_{\mathtt{G}}}\,\ell_{\mathtt{C}}(x_4)$ with the magnetic induction in the air gap $\phi_{\mathtt{PG}}/S_{\mathtt{G}}$ and the position-dependent effective wire length $\ell_{\mathtt{C}}(q_{\mathtt{D}})$ defined in (6). See definitions and notations in section 5.

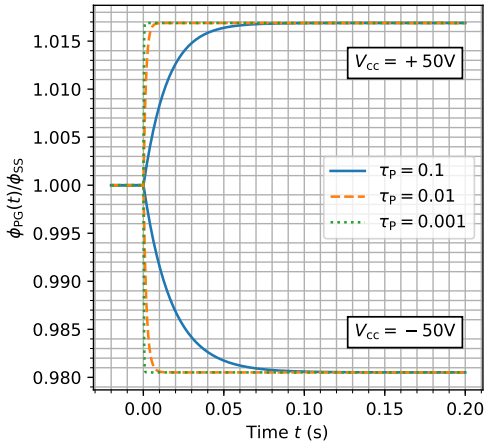

Figure 13: Simulation of the loudspeaker model 2 in table 4: Normalized flux $\frac{\phi_{\mathtt{PG}}}{\phi_{\mathtt{ss}}}$ in response to a ± 50V step voltage. The initial flux is $\phi_{\mathtt{PG}}(t=0) = \phi_{\mathtt{ss}}$ and the coil is blocked at $q_{\mathtt{D}} = 0$m. The sample-rate is 96kHz.

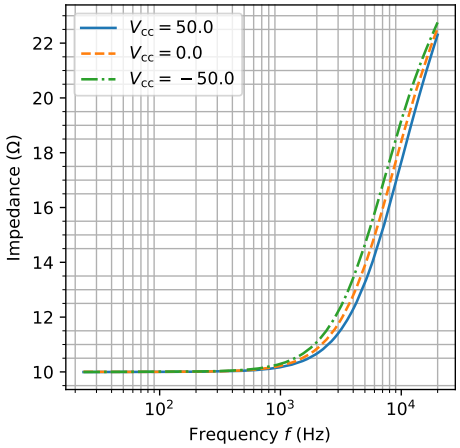

Figure 14: Simulation of the loudspeaker model 2 in table 4: Evolution of the modulus of impedance $\left|\frac{v_{\mathtt{I}}(2i\pi f)}{i_{\mathtt{C}}(2i\pi f)}\right|$ with the magnetic flux in the coil $\phi_{\mathtt{PG}}$ in response to a DC input voltage $v_{\mathtt{I}} = \mathcal{N}(V_{\mathtt{cc}}, 0.1)$ where $\mathcal{N}$ denotes the normal distribution centered on $V_{\mathtt{cc}}$ with variance 0.1V. The coil is blocked at $q_{\mathtt{D}} = 0$m. The sample-rate is 96kHz.

Flux-dependent force factor (phenomenon 2) The force factor in model 2 $B_\ell = \frac{\phi_{\mathtt{PG}}}{S_{\mathtt{G}}}\ell_{\mathtt{C}}(q_{\mathtt{D}})$ is modulated by the coil position (same as model 0) and the magnetic flux in the pole piece `P` and air gap `G`. This is clearly visible in the results of the figure 16: we observe that the force factor can be larger than predicted by the Thiele/Small modeling. Notice that the power balance is fulfilled.

6 Conclusion

In this paper, three lumped parameter models of the electrodynamic loudspeaker have been developed to incorporate refined phenomena of mechanical and electromagnetic origins. In particular, a finite-dimensional (power-balanced and) passive-guaranteed time-domain formulation of viscoelastic and eddy-currents phenomena (linear) and material properties (stress–strain and b–h characteristics, nonlinear) have been derived. Those models are given in the the framework of port-Hamiltonian systems, which decomposes the system into conservative, dissipative and source parts. The numerical method used for simulation preserves this decomposition

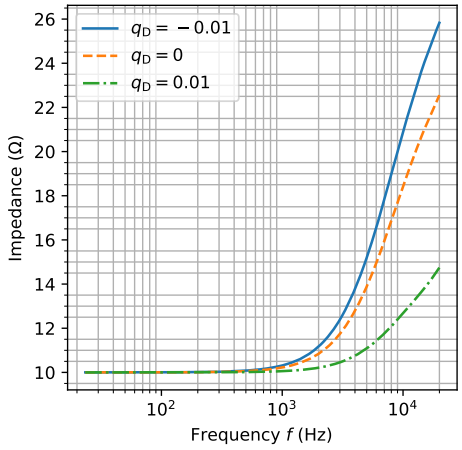

Figure 15: Simulation of the loudspeaker model 2 in table 4: Variation of impedance when the coil is blocked in different positions, hence changing the number of coil wire turns around the path $n_P(q_D)$ and the inductance according to (37). The flux is initially at $\phi_{PG}(t=0) = \phi_{ss}$. The sample-rate is 96kHz.

Numerical results that comply with measurements from the literature have been presented.

The three loudspeaker models 0, 1 and 2 have been developed independently of each other. This permits to illustrate the particular effect of each phenomenon on the loudspeaker dynamics. Now, their interconnection to form a global, multiphysical modeling that copes with all the phenomena described in section 2 is straightforward, due to the modularity of the port-Hamiltonian approach.

	Coupling			Mechanical		Electromagnetic	
	1	2	3	4	5	6	7
§3.3	✓						
§4	✓			✓	✓		
§5	✓	✓	✓			✓	✓

Table 5: Phenomena in section 2 addressed by each proposed port-Hamiltonian models: model 0 in §3.3, model 1 in §4 and model 2 in §5.

The first perspective of this work is to achieve DSP simulation-based real-time audio distortion compensation, based on the preliminary work in [14]. This requires the development of a parameter estimation method dedicated to the port-Hamiltonian structure. A second perspective is to include other phenomena that have not been considered here, such that the fractional dynamics associated with viscoelastic materials and eddy-currents, the acoustical load and the thermal evolution of the system. For all these issues, the modular structure of the proposed port-Hamiltonian models could be exploited in a further work.

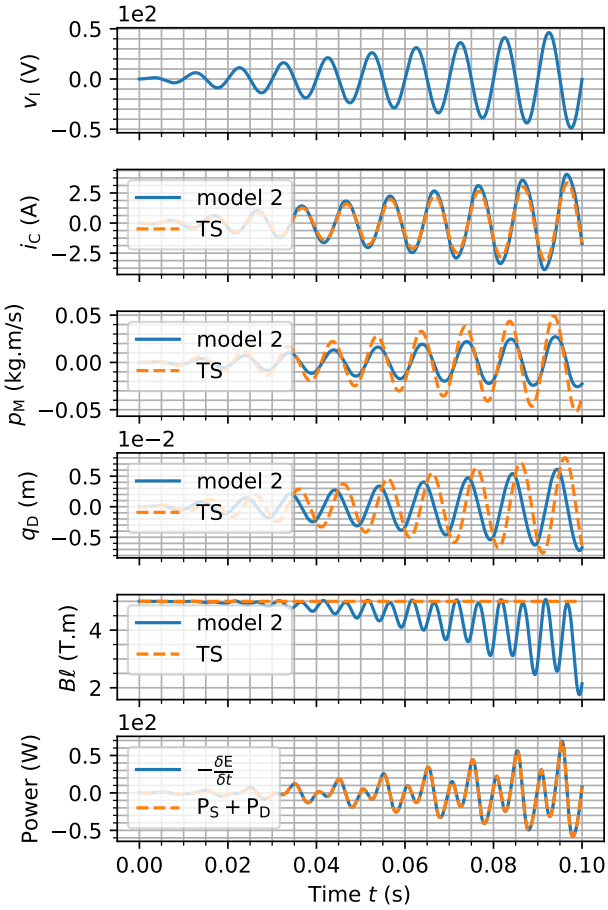

Figure 16: Simulation of the model 2 in table 4 depicted in figure 12, for the parameters in tables 6 and 8. The input voltage is a 100Hz sine wave with increasing amplitude between 0V and 50V. The sampling rate is 96kHz. The power balance is shown for the model 2 only. The force factor B_ℓ corresponds to the product of the induction in air gap b_G from (17) with position-dependent effective length from (6).

Acknowledgement

This work is supported by the project ANR-16-CE92-0028, entitled Interconnected Infinite-Dimensional systems for Heterogeneous Media, INFIDHEM, financed by the French National Research Agency (ANR). Further information is available at https://websites.isae-supaero.fr/infidhem/the-project The authors acknowledge Antonin Novak, Balbine Maillou (Laboratoire d´Acoustique de l´Université du Maine, UMR-CNRS 6613, Le Mans, France) for fruitful discussions on the loudspeaker mechanisms. The authors also acknowledge Robert Piéchaud for taking the time to complete the proofread of this paper.

References

[1] Finn T Agerkvist. Non-linear viscoelastic models. In *Audio Engineering Society Convention 131*. Audio Engineering Society, 2011.

[2] Finn T Agerkvist and Tobias Ritter. Modeling viscoelasticity of loudspeaker suspensions using retardation spectra. In *Audio Engineering Society Convention 129*. Audio Engineering Society, 2010.

[3] Marcus Arvidsson and Daniel Karlsson. Attenuation of harmonic distortion in loudspeakers using non-linear control. 2012.

[4] Mingsian R Bai and Chau-Min Huang. Expert diagnostic system for moving-coil loudspeakers using nonlinear modeling. *The Journal of the Acoustical Society of America*, 125(2):819–830, 2009.

[5] Samuel Brown. *Linear and Nonlinear Loudspeaker Characterization*. PhD thesis, Citeseer, 2006.

[6] Pascal Brunet. *Nonlinear System Modeling and Identification of Loudspeakers*. PhD thesis, Northeastern University Boston, 2014.

[7] Pascal Brunet and Bahram Shafai. State-space modeling and identification of loudspeaker with nonlinear distortion. In *Modelling, Identification, and Simulation, IASTED International Conference on*, volume 755, 2011.

[8] Pascal Brunet and Bahram Shafai. Identification of loudspeakers using fractional derivatives. *Journal of the Audio Engineering Society*, 62(7/8):505–515, 2014.

[9] R. Buntenbach. A generalized circuit model for multiwinding inductive devices. *Magnetics, IEEE Transactions on*, 6(1):65–65, March 1970.

[10] Peter John Chapman. Thermal simulation of loudspeakers. In *Audio Engineering Society Convention 104*. Audio Engineering Society, 1998.

[11] Mark Dodd, Wolfgang Klippel, and Jack Oclee-Brown. Voice coil impedance as a function of frequency and displacement. In *Audio Engineering Society Convention 117*. Audio Engineering Society, 2004.

[12] Vincent Duindam, Alessandro Macchelli, Stefano Stramigioli, and Herman Bruyninckx. *Modeling and Control of Complex Physical Systems: The Port-Hamiltonian Approach*. Springer Science & Business Media, 2009.

[13] Antoine Falaize and Thomas Hélie. Passive guaranteed simulation of analog audio circuits: A port-hamiltonian approach. *Applied Sciences*, 6(10):273, 2016.

[14] Antoine Falaize, Nicolas Papazoglou, Thomas Hélie, and Nicolas Lopes. Compensation of loudspeaker's nonlinearities based on flatness and port-Hamiltonian approach. In *22ème Congrès Français de Mécanique*, Lyon, France, August 2015. Association Française de Mécanique.

[15] William N Findley and Francis A Davis. *Creep and relaxation of nonlinear viscoelastic materials*. Courier Corporation, 2013.

[16] Vincent François-Lavet, François Henrotte, L Stainer, Ludovic Noels, and Christophe Geuzaine. Vectorial incremental nonconservative consistent hysteresis model. In *Proceedings of the 5th International Conference on Advanded COmputational Methods in Engineering (ACOMEN2011)*, 2011.

[17] Mathias Getzlaff. *Fundamentals of magnetism*. Springer Science & Business Media, 2007.

[18] D.C. Hamill. Lumped equivalent circuits of magnetic components: the gyrator-capacitor approach. *Power Electronics, IEEE Transactions on*, 8(2):97–103, Apr 1993.

[19] Sverre Holm, Sven Peter Näsholm, Fabrice Prieur, and Ralph Sinkus. Deriving fractional acoustic wave equations from mechanical and thermal constitutive equations. *Computers & Mathematics with Applications*, 66(5):621–629, 2013.

[20] Shuai Hu, Wen Chen, and Xiaofan Gou. Modal analysis of fractional derivative damping model of frequency-dependent viscoelastic soft matter. *Advances in Vibration Engineering*, 10(3):187–196, 2011.

[21] Toshiaki Itoh and Kanji Abe. Hamiltonian-conserving discrete canonical equations based on variational difference quotients. *Journal of Computational Physics*, 76(1):85–102, 1988.

[22] David Jakobsson and Marcus Larsson. Modelling and compensation of nonlinear loudspeaker. 2010.

[23] Arie JM Kaizer. Modeling of the nonlinear response of an electrodynamic loudspeaker by a volterra series expansion. *Journal of the Audio Engineering Society*, 35(6):421–433, 1987.

[24] Wolfgang Klippel. Dynamic measurement and interpretation of the nonlinear parameters of electrodynamic loudspeakers. *Journal of the Audio Engineering Society*, 38(12):944–955, 1990.

[25] Wolfgang Klippel. Nonlinear modeling of the heat transfer in loudspeakers. *Journal of the Audio Engineering Society*, 52(1/2):3–25, 2004.

[26] Wolfgang Klippel. Tutorial: Loudspeaker nonlinearities – causes, parameters, symptoms. *Journal of the Audio Engineering Society*, 54(10):907–939, 2006.

[27] Morten H Knudsen and J Grue Jensen. Low-frequency loudspeaker models that include suspension creep. *Journal of the Audio Engineering Society*, 41(1/2):3–18, 1993.

[28] RC Koeller. Applications of fractional calculus to the theory of viscoelasticity. *Journal of Applied Mechanics*, 51(2):299–307, 1984.

[29] Xiao-Peng Kong, Finn Agerkvist, and Xin-Wu Zeng. Modeling of lossy inductance in moving-coil loudspeakers. *Acta Acustica united with Acustica*, 101(3), 2015.

[30] Khosrow Lashkari. A novel volterra-wiener model for equalization of loudspeaker distortions. In *Acoustics, Speech and Signal Processing, 2006. ICASSP 2006 Proceedings. 2006 IEEE International Conference on*, volume 5, pages V–V. IEEE, 2006.

[31] Lionel Laudebat. Modélisation et identification sous représentation diffusive de comportements dynamiques non rationnels en génie électrique. *Thèse de l'Université Paul Sabatier, Toulouse*, 2003.

[32] W Marshall Leach Jr. Loudspeaker voice-coil inductance losses: circuit models, parameter estimation, and effect on frequency response. *Journal of the Audio Engineering Society*, 50(6):442–450, 2002.

[33] R Lewandowski and B Chorażyczewski. Identification of the parameters of the kelvin–voigt and the maxwell fractional models, used to modeling of viscoelastic dampers. *Computers & structures*, 88(1):1–17, 2010.

[34] Nicolas Lopes, Thomas Hélie, and Antoine Falaize. Explicit second-order accurate method for the passive guaranteed simulation of port-hamiltonian systems. *IFAC-PapersOnLine*, 48(13):223–228, 2015.

[35] BM Maschke, Arjan J Van Der Schaft, and Peter C Breedveld. An intrinsic hamiltonian formulation of network dynamics: Non-standard poisson structures and gyrators. *Journal of the Franklin institute*, 329(5):923–966, 1992.

[36] Bo Rohde Pedersen. *Error correction of loudspeakers*. PhD thesis, PhD thesis. Aalborg University, Denmark, 2008.

[37] Bo Rohde Pedersen and Finn T Agerkvist. Time varying behavior of the loudspeaker suspension. In *Audio Engineering Society Convention 123*. Audio Engineering Society, 2007.

[38] Axel Rumeau. *Modélisation comportementale en génie électrique sous représentation diffusive: méthodes et applications*. PhD thesis, Université de Toulouse, Université Toulouse III-Paul Sabatier, 2009.

[39] J Sabatier, Om P Agrawal, and JA Tenreiro Machado. *Advances in fractional calculus*, volume 4. Springer, 2007.

[40] Ingo Schäfer and Klaus Krüger. Modelling of lossy coils using fractional derivatives. *Journal of Physics D: Applied Physics*, 41(4):045001, 2008.

[41] Arjan Schaft. Port-hamiltonian systems: an introductory survey. 2006.

[42] Jean-Jacques E Slotine, Weiping Li, et al. *Applied nonlinear control*, volume 199. Prentice-hall Englewood Cliffs, NJ, 1991.

[43] Richard H Small. Closed-box loudspeaker systems-part 1: analysis. *Journal of the Audio Engineering Society*, 20(10):798–808, 1972.

[44] Richard H Small. Closed-box loudspeaker systems-part 2: Synthesis. *Journal of the Audio Engineering Society*, 21(1):11–18, 1973.

[45] Marcelo Soria-Rodríguez, Moncef Gabbouj, Nick Zacharov, Matti S Hämäläinen, and Kalle Koivuniemi. Modeling and real-time auralization of electrodynamic loudspeaker non-linearities. In *Acoustics, Speech, and Signal Processing, 2004. Proceedings.(ICASSP'04). IEEE International Conference on*, volume 4, pages iv–81. IEEE, 2004.

[46] Johan Suykens, Joos Vandewalle, and Johan Van Ginderdeuren. Feedback linearization of nonlinear distortion in electrodynamic loudspeakers. *Journal of the audio engineering society*, 43(9):690–694, 1995.

[47] Stéphan Tassart, Simon Valcin, and Michel Menu. Active loudspeaker heat protection. *Journal of the Audio Engineering Society*, 62(11):767–775, 2014.

[48] Neville Thiele. Loudspeakers in vented boxes: Part 1. *Journal of the Audio Engineering Society*, 19(5):382–392, 1971.

[49] Neville Thiele. Loudspeakers in vented boxes: Part 2. *Journal of the Audio Engineering Society*, 19(6):471–483, 1971.

[50] Knud Thorborg and Claus Futtrup. Frequency dependence of the loudspeaker suspension (a follow up). *Journal of the Audio Engineering Society*, 61(10):778–786, 2013.

[51] Knud Thorborg, Carsten Tinggaard, Finn Agerkvist, and Claus Futtrup. Frequency dependence of damping and compliance in loudspeaker suspensions. *Journal of the Audio Engineering Society*, 58(6):472–486, 2010.

[52] Knud Thorborg, Andrew D Unruh, and Christopher J Struck. An improved electrical equivalent circuit model for dynamic moving coil transducers. In *Audio Engineering Society Convention*, volume 122, 2007.

[53] John Vanderkooy. A model of loudspeaker driver impedance incorporating eddy currents in the pole structure. In *Audio Engineering Society Convention 84*. Audio Engineering Society, 1988.

[54] Julian R Wright. An empirical model for loudspeaker motor impedance. *Journal of the Audio Engineering Society*, 38(10):749–754, 1990.

A Numerical method

In this section, we present the numerical method used in this paper for the simulation of models 0, 1 and 2. It is based on the appropriate definition of a *discret gradient* [21] with restores the passive-guaranteed port-Hamiltonian structure (3) in discrete time so that numerical stability is guaranteed (see [34] for details).

To ensure stable simulation of stable dynamical system $\frac{\mathtt{d}\mathbf{x}}{\mathtt{d}t} = \mathbf{f}(\mathbf{x})$, many numerical schemes focus on the approximation quality of the time derivative, combined with operation of the vector field $\mathbf{f}$. Here, we adopt an alternative point of view, by transposing the power balance (4) in the discrete time-domain to preserve passivity. This is achieved by numerical schemes that provide a discrete version of the chain rule for computing the derivative of $\mathrm{E} = H \circ \mathbf{x}$. This is the case of Euler scheme, for which first order approximation of the differential applications $\mathtt{d}\mathbf{x}(t,\mathtt{d}t) = \frac{\mathtt{d}\mathbf{x}}{\mathtt{d}t}(t)\,\mathtt{d}t$ and $\mathtt{d}H(\mathbf{x},\mathtt{d}\mathbf{x}) = \nabla H(\mathbf{x})^\intercal\,\mathtt{d}\mathbf{x}$ on the sample grid $t = k\,\delta t$, $k \in \mathbb{Z}$ are given by

$$\begin{aligned} \delta\mathbf{x}(k,\delta t) &= \mathbf{x}(k+1) - \mathbf{x}(k), && (26)\\ \delta H\big(\mathbf{x},\delta\mathbf{x}\big) &= H\big(\mathbf{x}+\delta\mathbf{x}\big) - H\big(\mathbf{x}\big) && (27)\\ &= \nabla_d H\big(\mathbf{x},\mathbf{x}+\delta\mathbf{x}\big)^\intercal\,\delta\mathbf{x}. \end{aligned}$$

For mono-variate storage components ($H(\mathbf{x}) = \sum_{n=1}^{n_\mathbf{x}} H_n(x_n)$), the solution can be built element-wise with the n-th coordinate given by

$$[\nabla_d H\big(\mathbf{x},\mathbf{x}+\delta\mathbf{x}\big)]_n = \begin{cases} \frac{h_n\left(x_n+\delta x_n\right)-h_n\left(x_n\right)}{\delta x_n} & \text{if } \delta x_n \neq 0,\\ h_n'(x_n) & \text{otherwise.}\end{cases} \quad (28)$$

A discrete chain rule is indeed recovered

$$\frac{\delta\mathrm{E}(k,\delta t)}{\delta t} = \nabla^d H\big(\mathbf{x}(k),\mathbf{x}(k+1)\big)^\intercal\,\frac{\delta\mathbf{x}(k,\delta t)}{\delta t} \quad (29)$$

so that the following substitution in (3)

$$\begin{aligned} \tfrac{\mathtt{d}\mathbf{x}}{\mathtt{d}t}(t) &\to \tfrac{\delta\mathbf{x}(k,\delta t)}{\delta t}\\ \nabla\mathrm{H}(\mathbf{x}) &\to \nabla^d H\big(\mathbf{x}(k),\mathbf{x}(k+1)\big)\end{aligned} \quad (30)$$

leads to

$$\begin{aligned} 0 &= \mathbf{a}(k)^\intercal\,\mathbf{J}\,\mathbf{a}(k) = \mathbf{a}(k)^\intercal\,\mathbf{b}(k)\\ &= \underbrace{\left[\nabla^d H^\intercal\,\frac{\delta\mathbf{x}}{\delta t}\right](k)}_{\frac{\delta\mathrm{E}(k,\delta t)}{\delta t}} + \underbrace{\mathbf{z}(\mathbf{w}(k))^\intercal\mathbf{w}(k)}_{\mathrm{P_D}(k)} - \underbrace{\mathbf{u}(k)^\intercal\mathbf{y}(k)}_{\mathrm{P_S}(k)}. \end{aligned} \quad (31)$$

For pH systems composed of a collection of linear energy storing components with quadratic Hamiltonian $H_n(x_n) = \frac{x_n^2}{2C_n}$, we define $\mathbf{Q} = \mathrm{diag}(C_1 \cdots C_{n_\mathbf{x}})^{-1}$ so that the discrete gradient (28) reads

$$\nabla^d H\big(\mathbf{x},\mathbf{x}+\delta\mathbf{x}\big) \;=\; \mathbf{Q}\left(\mathbf{x}(k) + \tfrac{\delta\mathbf{x}(k)}{2}\right), \quad (32)$$

which restores the midpoint rule. For nonlinear case, (28) leads to another numerical scheme depending on the nonlinearity, still preserving passivity.

B Recalls on magnetism

In this section, we give the elements for the modeling of lumped electromagnetic systems in the pH formalism. First, the closed-form expression for energy storage is recalled Second and third, we give the port-Hamiltonian formulation of electromechanical and electromagnetic coupling, respectively.

B.1 Magnetic energy storage

Definitions The magnetic phenomena are described by two complementary fields, namely, the applied magnetic excitation $\mathbf{h}$ and the induced magnetic flux density $\mathbf{b}(\mathbf{h})$, which is somewhat the response of a given material to a given excitation. The induction $\mathbf{b}$ is defined as the superposition of the magnetization of vacuum $\mathbf{j}_0(\mathbf{h})$ and the magnetization of matter $\mathbf{j}(\mathbf{h})$ due to microscopic magnetic moments attached to the atoms of the body (see [17, (1.6)] and [16, (6)]):

$$\mathbf{b} = \mathbf{j}_0(\mathbf{h}) + j(\mathbf{h}) \simeq j(\mathbf{h})$$

where we neglect the magnetization of vacuum so that $\mathbf{h}(\mathbf{b}) = \mathbf{j}^{-1}(\mathbf{b})$. The magnetic induction flux ϕ is defined as the flux of the magnetic induction

field through a given surface $\mathcal{S}$: $\phi(t) = \iint_{\mathcal{S}} b(t)\,\mathtt{d}S = S\,b(t)$, where we assumed $b(t)$ constant over $\mathcal{S}$. The *magnetomotive force* ψ is defined as the circulation of $\mathbf{h}$ along a closed $\mathbf{b}$-field line $\mathcal{C}$ with length $\ell_{\mathcal{C}}$: $\psi\big(b(t)\big) = \oint_{\mathcal{C}} h\big(b(t)\big)\,\mathtt{d}\ell = \ell_{\mathcal{C}}.h\big(b(t)\big)$, where we assumed $h\big(b(t)\big)$ constant along $\mathcal{C}$.

Energy storage The variation of magnetic energy density stored in a sample of magnetic material is $\frac{\mathtt{d}\mathcal{E}}{\mathtt{d}t} = h(b)\frac{\mathtt{d}b}{\mathtt{d}t}$ (see *e.g.* [16] for details). The total energy variation for a sample with length $\ell_{\mathcal{C}}$ and section S (m^2) is then $\frac{\mathtt{d}E}{\mathtt{d}t} = S\,\ell\,h(b)\frac{\mathtt{d}b}{\mathtt{d}t} = \psi\left(\frac{\phi}{S}\right)\frac{\mathtt{d}\phi}{\mathtt{d}t}$. The associated storage function (Hamiltonian) is defined by

$$\mathrm{H}_{\mathtt{mag}}(\phi) = \ell_{\mathcal{C}} \int_0^{\phi} h\left(\frac{x}{S}\right)\mathtt{d}x \tag{33}$$

which restores the total energy variation $\frac{\mathtt{d}}{\mathtt{d}t}\mathrm{H}_{\mathtt{mag}} = \psi\,\frac{\mathtt{d}\phi}{\mathtt{d}t}$.

B.2 Electromechanical coupling

Consider several windings of a conductive wire with section $S_{\mathtt{W}}$, length $\ell_{\mathtt{W}}$, position $q_{\mathtt{W}}$ and velocity vector $\mathbf{v}_{\mathtt{W}} = \mathrm{v}_{\mathtt{W}}\,\mathbf{e}_{\mathtt{W}}$ with constant direction $\mathbf{e}_{\mathtt{W}}$ and magnitude $\mathrm{v}_{\mathtt{W}} = \frac{\mathtt{d}q_{\mathtt{W}}}{\mathtt{d}t}$. This conductor is immersed in a magnetic induction field $\mathbf{b}$ with constant direction orthogonal to $\mathbf{e}_{\mathtt{W}}$ and constant magnitude B. The current is $i_{\mathtt{W}} = \iint_{S_{\mathtt{W}}} \rho_q\,\mathbf{v}_q \mathtt{d}S$ for the electric charge density ρ_q moving with velocity $\mathbf{v}_q = \mathrm{v}_q\,\mathbf{e}_q$ and unitary vector $\mathbf{e}_q$ normal to the surface $S_{\mathtt{W}}$. A wire element with length $\mathtt{d}\ell$ is subjected to the Lorentz force $\mathtt{d}\mathbf{f}_{\mathcal{L}} = \rho_q\,S_{\mathtt{W}}\,\mathtt{d}\ell\;(\mathbf{v}_q + \mathbf{v}_{\mathtt{W}}) \times \mathbf{b}$. This force is orthogonal to the velocity $\mathbf{v}_q + \mathbf{v}_{\mathtt{W}}$ so that the associated mechanical power is $\mathtt{d}\mathrm{P}_{\mathcal{L}} = \mathtt{d}\mathbf{f}_{\mathcal{L}} \cdot (\mathbf{v}_q + \mathbf{v}_{\mathtt{W}}) = 0$. Integrating along the wire, one gets

$$\mathrm{P}_{\mathcal{L}} = \mathrm{v}_{\mathtt{W}}.\underbrace{B\,\ell_{\mathtt{W}}\,i_{\mathtt{W}}}_{f_{\mathcal{L}}} + i_{\mathtt{W}}\underbrace{B\,\ell_{\mathtt{W}}\,\mathrm{v}_{\mathtt{W}}}_{v_{\mathcal{L}}} = 0 \tag{34}$$

defining the Lorentz force $f_{\mathcal{L}}$ and the back electromotive force (voltage) $v_{\mathcal{L}}$. Notice the transfer is reversible and conservative in the sense that the outflow of energy from the electrical domain $\mathrm{P}_{\mathtt{elec}} = i_{\mathtt{W}}\,v_{\mathcal{L}}$ equals the inflow of the mechanical domain $\mathrm{P}_{\mathtt{meca}} = \mathrm{v}_{\mathtt{W}}\,f_{\mathcal{L}}$, that is $\mathrm{P}_{\mathcal{L}} = \mathrm{P}_{\mathtt{meca}} - \mathrm{P}_{\mathtt{elec}} = 0$. This corresponds to a gyrator with ratio $B\,\ell_{\mathtt{W}}$:

$$\begin{pmatrix} v_{\mathcal{L}} \\ f_{\mathcal{L}} \end{pmatrix} = \begin{pmatrix} 0 & -B\,\ell_{\mathtt{W}} \\ B\ell_{\mathtt{W}} & 0 \end{pmatrix} \cdot \begin{pmatrix} i_{\mathtt{W}} \\ \mathrm{v}_{\mathtt{W}} \end{pmatrix}. \tag{35}$$

B.3 electromagnetic coupling: the gyrator-capacitor approach

The gyrator-capacitor approach introduced in the late sixties [9, 18] is an easy way to develop electronic analog of magnetic circuits. It has been considered in [32] for the modeling of the loudspeaker. In this approach, a coil is divided in a gyrator (wire turns) and a magnetic energy storage (coil core).

The dynamics of a magnetic field can be described by two complementary macroscopic quantities: the *magnetic induction field* ψ and the *magnetomotive force* (mmf) ψ (see B.1). The electromagnetic transfer for a single wire turn stands from (i) *Faraday's law* of electromagnetic induction that relates the electromotive force (tension v) to the variation of the magnetic flux in the wire turn $v = \frac{\mathtt{d}\phi}{\mathtt{d}t}$; and (ii) *Ampère's theorem* that relates the mmf to the current in the wire $\psi = i$ [9, 18]. Considering the coil ($\mathtt{C}$) in figure **??** with $N_{\mathtt{C}}$ wire turns around the path ($\mathtt{P}$), these relations restores a gyrator with ratio $N_{\mathtt{C}}$:

$$\begin{pmatrix} v_{\mathtt{C}} \\ \psi_{\mathtt{C}} \end{pmatrix} = \begin{pmatrix} 0 & N_{\mathtt{C}} \\ N_{\mathtt{C}} & 0 \end{pmatrix} \begin{pmatrix} i_{\mathtt{C}} \\ \frac{\mathtt{d}\phi_{\mathtt{C}}}{\mathtt{d}t} \end{pmatrix}. \tag{36}$$

Denoting by $s \in \mathbb{C}$ the Laplace variable, the correspondence between an impedance seen in the electrical domain $\mathcal{Z}_{\mathtt{elec}}(s) = \frac{v_{\mathtt{C}}(s)}{i_{\mathtt{C}}(s)}$ and its counterpart in the magnetic domain $\mathcal{Z}_{\mathtt{mag}}(s) = \frac{\psi_{\mathtt{C}}(s)}{s\,\phi_{\mathtt{C}}(s)} = \frac{N_{\mathtt{C}}^2\,i_{\mathtt{C}}(s)}{v_{\mathtt{C}}(s)}$ is given by

$$\mathcal{Z}_{\mathtt{mag}}(s) = \frac{N_{\mathtt{C}}^2}{\mathcal{Z}_{\mathtt{elec}}(s)}, \tag{37}$$

so that the electrical inductance associated with the magnetic capacity is $L_{\mathtt{C}} = N_{\mathtt{C}}^2\,C_{\mathtt{P}}$. Notice the interconnection (36) is conservative: $\mathrm{P}_{\mathtt{elec}} = \mathrm{P}_{\mathtt{mag}}$ with $\mathrm{P}_{\mathtt{elec}} = v_{\mathtt{C}}\,i_{\mathtt{C}}$ the power outgoing the electrical domain and $\mathrm{P}_{\mathtt{mag}} = \frac{\mathtt{d}\phi_{\mathtt{C}}}{\mathtt{d}t}\,\psi_{\mathtt{C}}$ the power incoming the magnetic domain.

C State saturating storage function

The saturation effect of the suspension (phenomenon 5) and the ferromagnetic path (phenomenon 6) are described by the same idealized (symmetric) saturation curve $c(x)$. It is built as the linear combination of basis functions $c_{\mathtt{lin}}(x)$ (linear behavior around the origin) and $c_{\mathtt{sat}}(x)$ (saturation effect):

$$c(x) = P_{\mathtt{lin}}(c_{\mathtt{lin}}(x) + P_{\mathtt{sat}}c_{\mathtt{sat}}(x))\,, \tag{38}$$

$$c_{\mathtt{lin}}(x) = x, \tag{39}$$

$$c_{\mathtt{sat}}(x) = \frac{4}{4-\pi}\left(\tan\left(\frac{\pi.x}{2\,x_{\mathtt{sat}}}\right) - \frac{\pi.x}{2x_{\mathtt{sat}}}\right) \tag{40}$$

with $c_{\mathtt{sat}}(x) \xrightarrow{x\to\pm x_{\mathtt{sat}}} \pm\infty$, $\frac{\partial c_{\mathtt{sat}}}{\partial x}(0) = 0$ so that $c_{\mathtt{sat}}(x)$ does not contribute around origin, and $c_{\mathtt{sat}}\left(\frac{1}{2}\right) = 1$.

The corresponding Hamiltonian is obtained from

$$\mathrm{H}(x) = \int_0^x c(\xi)\,\mathtt{d}\xi = P_{\mathtt{lin}}\left(H_{\mathtt{lin}}(x) + P_{\mathtt{sat}}H_{\mathtt{sat}}(x)\right) \tag{41}$$

with

$$\begin{aligned} H_{\mathtt{lin}}(x) &= \tfrac{x^2}{2}, \\ H_{\mathtt{sat}}(x) &= -\tfrac{8x_{\mathtt{sat}}}{\pi(4-\pi)}\left(\ln\left|\cos\left(\tfrac{\pi\,x}{2\,x_{\mathtt{sat}}}\right)\right| + \tfrac{1}{2}\left(\tfrac{\pi\,x}{2x_{\mathtt{sat}}}\right)^2\right). \end{aligned} \tag{42}$$

This nonlinear saturating storage function proves positive definite providing the parameters $(P_{\mathtt{lin}}, P_{\mathtt{sat}})$ are positive, so that it can be used in structure (3), still preserving passivity.

D Physical and technological parameters

Acronym *d.u.* stands for *dimensionless unit.*

Label	Description	Value	Unit
$R_{\mathtt{C}}$	Coil wire resistance	10	Ω
$L_{\mathtt{C}}$	Coil self inductance	3.10^{-4}	H
${\ell_{\mathtt{C}}}^0$	Coil wire length	10	m
$M_{\mathtt{CDA}}$	Total moving mass	10^{-2}	Kg
$K_{\mathtt{SA}}$	Total stiffness	2.10^3	$\mathrm{N.m^{-1}}$
$R_{\mathtt{SA}}$	Damping	1	$\mathrm{N.s.m^{-1}}$
B_ℓ	Force factor	5	T.m
B	Magnetic induction	${B_\ell}/{\ell_{\mathtt{C}}}^0$	T
Q_ℓ	Overhang in (6)	5.10^{-3}	m
P_ℓ	Shape in (6)	5	*d.u.*

Table 6: Physical and technological parameters involved in the model 0 of table 1. Typical values are chosen in accordance with data provided in [36, table 3.1] for the DALI 311541 $6\,1/2''$ unit.

Label	Description	Value	Unit
$\tau_{\mathtt{ve}}$	Creep time	1	s
P_K	Parameter in (11)	0.5	*d.u.*
$q_{\mathtt{sat}}$	Saturation position	10^{-2}	m
$P^{\mathtt{S}}_{\mathtt{sat}}$	Nonlinearity coefficient	10	*d.u.*
K_0	Primary stiffness	$\frac{K_{\mathtt{SA}}}{1-P_K}$	$\mathrm{N.m^{-1}}$
ω_1	Creep frequency	$\frac{2\pi}{\tau_{\mathtt{ve}}}$	Hz
K_1	Creep stiffness	$\frac{K_{\mathtt{SA}}}{P_K}$	$\mathrm{N.m^{-1}}$
R_1	Creep damping	$\frac{K_1}{\omega_1}$	$\mathrm{N.s.m^{-1}}$

Table 7: Physical and technological parameters involved in creep model in model 1 of table 3. Typical values are chosen in accordance with [51, table 1].

Label	Description	Value	Unit
$N_{\mathtt{C}}$	Wire turns	100	*d.u.*
$A_{\mathtt{C}}$	Coil height	2×10^{-2}	m
$D_{\mathtt{C}}$	Coil diameter	2.10^{-2}	m
$\tau_{\mathtt{ec}}$	Eddie-currents time	10^-4	s
μ_0	Vacuum permeability	$4\,\pi\,10^{-7}$	$\mathrm{H.m^{-1}}$
$\xi_{\mathtt{air}}$	Air susceptibility	3.6×10^{-7}	*d.u.*
$L_{\mathtt{P}}$	Path inductance	$L_{\mathtt{C}} - L_{\mathtt{leak}}$	H
$S_{\mathtt{G}}$	Air gap flux area	$\pi\,D_{\mathtt{C}}\,A_{\mathtt{C}}$	$\mathrm{m^2}$
$S_{\mathtt{P}}$	Pole piece flux area	$S_{\mathtt{G}}$	$\mathrm{m^2}$
$\alpha_{\mathtt{leak}}$	Leakage area ratio	10^{-2}	*d.u.*
$S_{\mathtt{leak}}$	Leakage area	(15)	$\mathrm{m^2}$
$\psi_{\mathtt{M}}$	Magnet mmf	(20)	A
$\phi_{\mathtt{ss}}$	Steady-state flux	$\frac{B}{S_{\mathtt{P}}}$	Wb
$L_{\mathtt{leak}}$	Leakage inductance	§5.1	H

Table 8: Physical and technological parameters involved in the model 2 of table 4. Typical values are chosen in accordance with [52, table 3].